

QC
807.5
.U66
no. 453
c.2

NOAA Technical Memorandum ERL 453-ETL 67



Measurement of Property Gradients and Turbulence Aloft With Ground-Based Doppler Radars

Earl E. Gossard
Richard G. Strauch
B. Boba Stankov
Daniel E. Wolfe

August 1995

U.S. DEPARTMENT OF COMMERCE
National Oceanic and Atmospheric Administration
Environmental Research Laboratories

QC
807.5
.466
110.453
10-27
C 2



Measurement of Property Gradients and Turbulence Aloft With Ground-Based Doppler Radars

Earl E. Gossard
Cooperative Institute for Research in Environmental Sciences

Richard G. Strauch
Cooperative Institute for Research in Environmental Sciences

B. Boba Stankov
Environmental Technology Laboratory

Daniel E. Wolfe
Environmental Technology Laboratory



Environmental Technology Laboratory
Boulder, Colorado

August 1995

U.S. Department of Commerce
Ronald H. Brown, Secretary

National Oceanic and Atmospheric Administration
D. James Baker, Under Secretary for Oceans and Atmosphere/Administrator

Environmental Research Laboratories
Silver Spring, Maryland
James L. Rasmussen, Director

NOTICE

Mention of a commercial company or product does not constitute an endorsement by NOAA/Environmental Research Laboratories. Use of information from this publication concerning proprietary products or the tests of such products for publicity or advertising purposes is not authorized.

For sale by the National Technical Information Service, 5285 Port Royal Road
Springfield, VA 22061

Contents

Abstract	1
1. INTRODUCTION	1
2. OBSERVATIONS	4
2.1. Tower Observations	4
2.2. Radar Observations	7
3. C_w^2 PROFILES	8
3.1. Calculation of C_w^2	8
3.2. Experimental Comparison of C_w^2 Retrievals With Measured Spectra	9
3.3. Turbulence Profile Retrieval on 26 May 1994	11
4. REFRACTIVE INDEX AND HUMIDITY RETRIEVAL OF 26 MAY 1994	13
5. CONCLUSIONS	18
6. REFERENCES	18
Appendix	23
A.1. INTRODUCTION	23
A.2. REFRACTIVE INDEX OF MICROWAVE FREQUENCIES	26
A.3. RADAR SENSING OF THE GRADIENT QUANTITIES	28
A.4. HUMIDITY RETRIEVAL	31

Measurement of Property Gradients and Turbulence Aloft With Ground-Based Doppler Radars

Earl E. Gossard, Richard G. Strauch, B. Boba Stankov, and Daniel E. Wolfe

Abstract. Results are described of an experiment to test the accuracy of a radar technique for calculating height profiles of turbulent dissipation rate and structure parameters in the clear air. The technique uses the second moment of the Doppler spectrum of backscatter from refractive index turbulence fluctuations. Such remote sensing of turbulence by present state-of-the-art wind profilers would allow routine monitoring of profiles of the intensity of turbulence and its outer scale throughout the lower atmosphere. The experiment lends support to the accuracy of the technique. If the accuracy is confirmed by further experiments, it would also, in principle, allow wind profilers to monitor the height gradients of refractive index in elevated layers and, if accompanied by a Radio Acoustic Sounding System, to extract the associated humidity gradients.

1. INTRODUCTION

Doppler radar wind profilers (e.g., Strauch et al., 1984) measure the radial velocity spectrum of target movement in the pulse volume. The first moment of the spectrum provides the mean radial velocity toward or away from the radar, thus giving the wind and wind shear profiles for which radar wind profilers were primarily designed. When the radars are pointing vertically, the second moment (or width) of the spectrum contains information about the vertical component w of the turbulent velocity fluctuations, i.e., the turbulent dissipation rate ϵ and structure parameter C_w^2 within the pulse volume. The theory and practice of using the spectral width to calculate the structure parameter of the turbulent velocity field (C_w^2 for the vertical velocity component w) was discussed by Gorelik and Mel' nichuk (1963), Srivastava and Atlas (1972), Frisch and Clifford (1974), Strauch and Merrem (1976), Lobbitt (1981), Gossard et al. (1982), Gossard and Strauch (1983), Hocking (1983), and Doviak and Zrnić (1984).

From the zero moment of the spectrum, i.e., the radar backscattered power from clear-air refractive index turbulence (RIT), the structure parameter of turbulent refractive index fluctuations, C_ϕ^2 , can be calculated. The relevant equations and the experiments establishing the reliability of such calculations are given in the Appendix.

For isotropic homogeneous turbulence in a horizontally homogeneous medium with vertical gradients of mean properties, Gossard et al. (1982) showed [Eq. (30)] that

$$\frac{C_\theta^2}{(d\theta_0/dz)^2} \frac{(du_0/dz)^2}{C_w^2} = \frac{B_\theta}{B_w} \left[\frac{K_m}{K_\theta} - \text{Ri} \right]^{-1}, \quad (1)$$

where θ_0 is the unperturbed potential temperature, C_θ^2 is the structure parameter of potential temperature, u_0 is the unperturbed horizontal wind, B_θ and B are Kolmogorov constants given in Table 1, and $B_w = 4/3B$. (Note in Table 1 that ϕ represents any passive scalar as well as potential temperature.) K_m and K_θ are the eddy coefficients of momentum and temperature, respectively, and their ratio is the turbulent Prandtl number Pr . $\text{Ri} = \omega_B^2/(du_0/dz)^2$ is the gradient Richardson number, and $\omega_B = [(g/\theta_0)(d\theta_0/dz)]^{0.5}$ is the Väisälä-Brunt frequency, where g is gravitational acceleration. Some form of (1) has been used by several researchers (e.g., VanZandt et al., 1978; Gage et al., 1980; Warnock and VanZandt, 1985) assuming various values for Ri and K_m/K_θ . Gossard et al. (1982) pointed out that the

Table 1. Turbulence parameters.

Relationship	Range of Values
<i>Velocity Field</i>	
$E(k) = \alpha \epsilon^{2/3} k^{-5/3}$	$\alpha = 1.53-1.68$
$S(k_1) = A \epsilon^{2/3} k_1^{-5/3}$	$A = 0.50-0.55$
$D_u(l) = \overline{[u(x+l) - u(x)]^2} = \underbrace{B \epsilon^{2/3} l^{2/3}}_{C_\epsilon^2}$	$B = 2.0-2.2$
<i>Potential Refractivity Field ϕ</i> (Also Potential Temperature and Other Passive Scalar Fields)	
$E_\phi(k) = \alpha_\phi \epsilon^{-1/3} \epsilon_\phi k^{-5/3}$	$\alpha_\phi = 1.33-1.67$
$S_\phi(k_1) = A_\phi \epsilon^{-1/3} \epsilon_\phi k_1^{-5/3}$	$A_\phi = 0.8-1.0$
$D_\phi(l) = \underbrace{B_\phi \epsilon^{-1/3} \epsilon_\phi l^{2/3}}_{C_\phi^2}$	$B_\phi = 3.2-4.0$

left side of (1) can be expressed as a ratio of length scales to the 4/3 power; i.e.

$$L_\theta^{4/3} = C_\theta^2 \left[\frac{d\theta_0}{dz} \right]^{-2} \quad \text{and} \quad L_w^{4/3} = C_w^2 \left[\frac{dw_0}{dz} \right]^{-2} \quad (2)$$

L_θ and L_w are variously referred to as outer scales or vertical mixing lengths (e.g., Tatarskii, 1971, p. 73). Obviously the two lengths, L_θ and L_w , will not, in general, be the same. Furthermore, both will depend on stability (expressed by the Richardson number) and be reduced under stable conditions because the eddy structure will be flattened by the work done against buoyancy in moving vertically. However, Gossard et al. (1982) suggested that their *ratio should be nearly constant*, because both heat and momentum are mixed by the same eddy ensemble.

Because w is the convenient wind component to measure by radar, whereas the horizontal wind u is used for shear, Eq. (1) assumes that the redistribution of momentum among velocity components takes place fast enough that isotropy essentially exists for those scales important to the experiment.

From the same reasoning that led to Eq. (1), it can be shown that similar relationships between structure parameters and gradients hold for other passive scalars having the same spectral form. In particular, considerable effort has been devoted to justification of the conclusion that the potential refractivity ϕ (see the Appendix) has the same spectral form as θ and humidity q (Andreas, 1987; Hill, 1989). It is Eq. (1), with θ replaced by ϕ , that is of interest here.

Gossard et al. (1984a) reported measurements (see the Appendix) within a stable layer that rose across a suite of fast-response in situ sensors at 175-m altitude on a meteorological tower at Erie,

Colorado. These measurements supported the equality $L_\theta = L_q = L_\phi \equiv (1.3 \pm 0.1) L_w$ (see Appendix, Fig. A2) where q is specific humidity, ϕ is potential refractive index, and w is the vertical component of the velocity. Then substituting ϕ for θ in (1), we find the height gradient of refractivity to be given by

$$\left(\frac{d\phi_0}{dz} \right)^2 = 0.7 \left(\frac{du_0}{dz} \right)^2 \frac{C_\phi^2}{C_w^2}, \quad (3a)$$

and a relationship between Ri and K provided by

$$\left(\frac{K_m}{K_\phi} Ri \right)^{-1} = 0.7 \frac{B_w}{B_\phi}. \quad (3b)$$

Equations of the form (3a) can be derived in a variety of ways: from the flux equation (Gossard and Sengupta, 1988), from the energy equation (Gage et al., 1980; Gossard et al., 1982), and from mixing length concepts (Tatarskii, 1971). However, as pointed out by Gossard et al. (1982), the form of (3b) suggests a deeper physical significance and provides a simple relationship between the Richardson number and K_m/K_ϕ (equivalent to the turbulent Prandtl number). Thus, (3a) provides a convenient relationship for calculating the gradient of mean ϕ from Doppler radar observations, if C_ϕ^2 , du_0/dz , and C_w^2 can be provided by the zero, first, and second moments of the spectra of backscatter from Doppler wind profilers; furthermore, (3b) provides a simple relation between Ri and Pr that is in good agreement with observations [see Fig. 1, adapted from Kondo et al. (1978)].

With vertically pointing systems equipped with a Radio Acoustic Sounding System (RASS; i.e., temperature but no winds), it may be convenient to express (3a) in terms of the Richardson number and the Väisälä-Brunt frequency ω_B [Gossard and Sengupta, 1988, Eq. (24)]; i.e.,

$$\left(\frac{d\phi_0}{dz} \right)^2 = C_1 \omega_B^2 \frac{C_\phi^2}{C_w^2}, \quad (4)$$

where $C_1 \approx 0.7 (B_w/B_\phi) Ri^{-1}$ and $\omega_B^2 = (g/\theta_0)(d\theta_0/dz)$. Equation (4) is useful when constraints on Ri (e.g., $Ri = 0.25$) are to be examined.

[We note here that measurements of $\overline{w^2/\phi^2}$ equal C_w^2/C_ϕ^2 in the inertial subrange at scales for which the spectra of w and ϕ have the same form (e.g., $k^{-5/3}$). The quantities w and ϕ are henceforth defined to be the perturbation quantities; the unperturbed quantities have zero subscripts. Considerable effort has been devoted to the justification of the conclusion that ϕ has the same spectral form as θ and q (Andreas, 1987; Hill, 1989).]

Finally, if temperature profiles are available from RASS, profiles of the humidity gradient dq_0/dz can be found [see Appendix, Eq. (A11)] from

$$\frac{dq_0}{dz} = \frac{\partial \phi^{-1}}{\partial q} \left[\frac{d\phi_0}{dz} - \frac{\partial \phi}{\partial \theta} \frac{d\theta_0}{dz} \right]. \quad (5)$$

For meteorological purposes, profiles of gradients are not as interesting as profiles of mean quantities such as temperature and humidity. However, if algorithms used in radiometric retrieval are constrained by given gradients and thicknesses at known altitudes, detailed structure can be retrieved (Stankov et al., 1995). On 26 May 1994, the date analyzed in this paper, the Denver balloon sounding shown in Fig. 2, had a pronounced humidity gradient near the 560-mb level. To test the concept, we carried out the usual

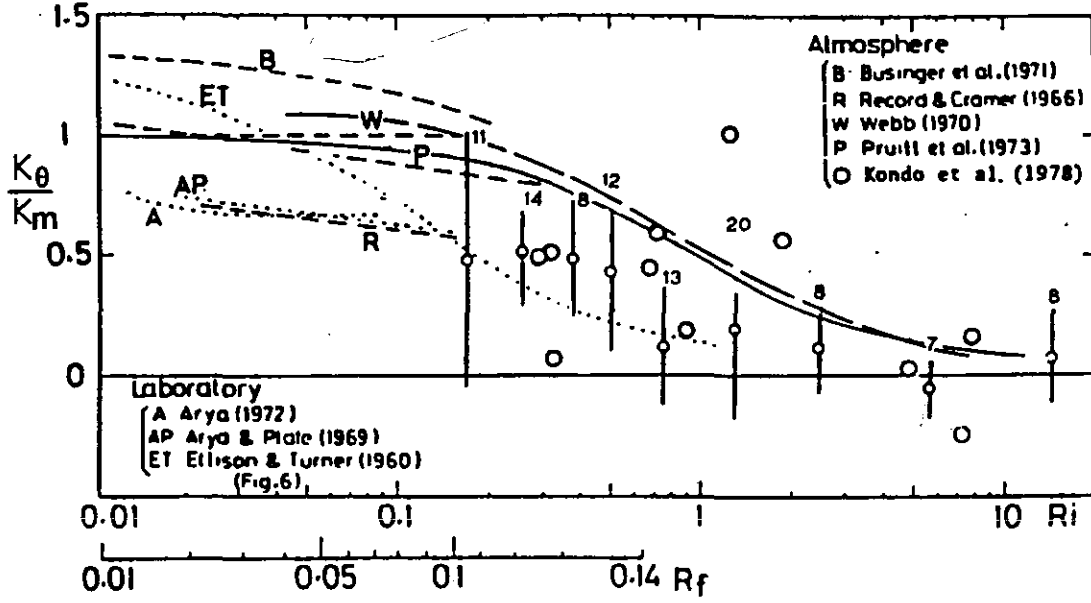


Figure 1. Compilation of data from many workers, by Kondo et al. (1978), showing the relationship between the inverse turbulent Prandtl number K_θ/K_m and the Richardson number Ri . The small and large circles indicate 2-min and 30-min runs, respectively, by Kondo et al. The light short-dashed lines are other field results, and the dotted lines are laboratory results. The heavy solid and heavy long-dashed lines are theoretical results from Eq. (3b) of the present paper. For references to specific data sets, see Kondo et al. (1978).

retrieval using radiometric and climatological data. The resulting dewpoint profile is shown plotted in Fig. 3 (dashed curve). The heavy solid curve resulted when the gradient information at the 560-mb level was added as a constraint. The agreement with the in situ radiosonde result (light solid curve) is seen to be much improved by the gradient information, which can, in principle, be provided by the radar.

2. OBSERVATIONS

2.1. Tower Observations

Instrumented towers offer the potential for directly measuring relationships such as (1), because by definition

$$\overline{[\theta(r) - \theta(r+l)]^2} = C_\theta^2 l^{2/3}, \quad (6a)$$

and

$$\overline{[w(r) - w(r+l)]^2} = C_w^2 l^{2/3}, \quad (6b)$$

where r is position and l is the sensor separation. The overbar means average. So the structure parameters can be measured directly from time-lagged measurements by fast-response sensors of θ and w or by

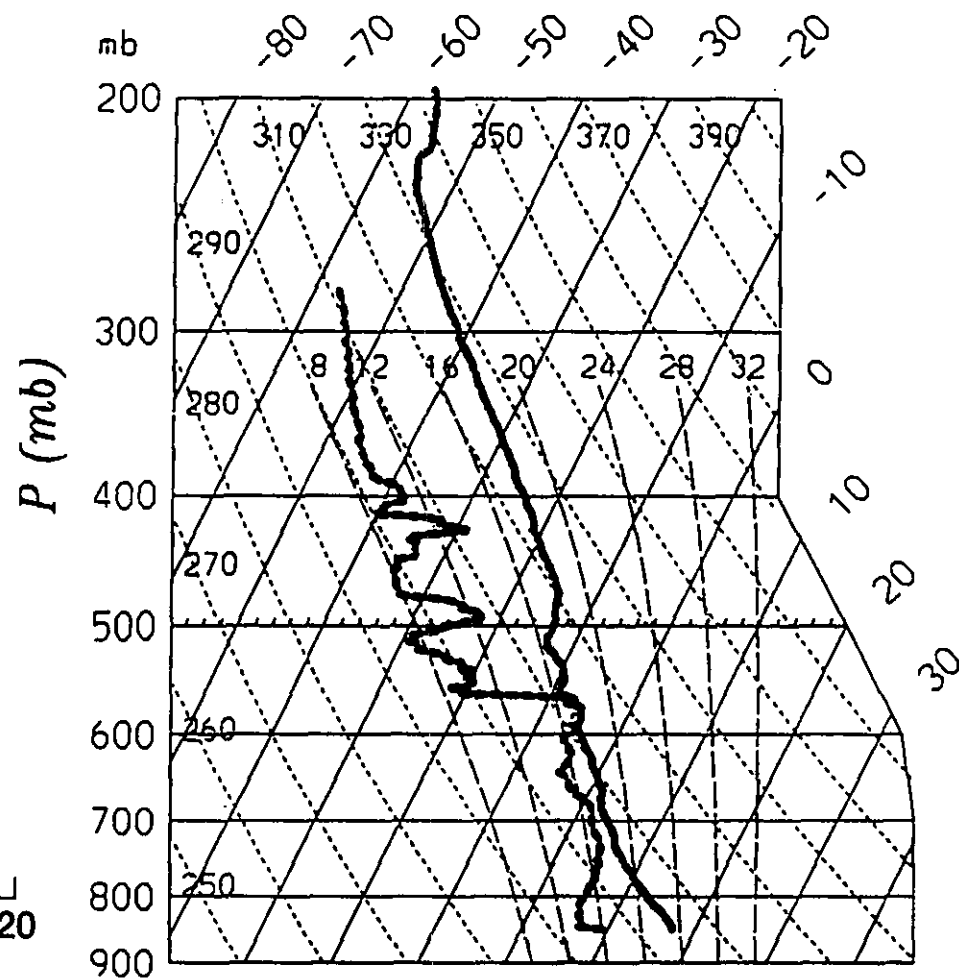
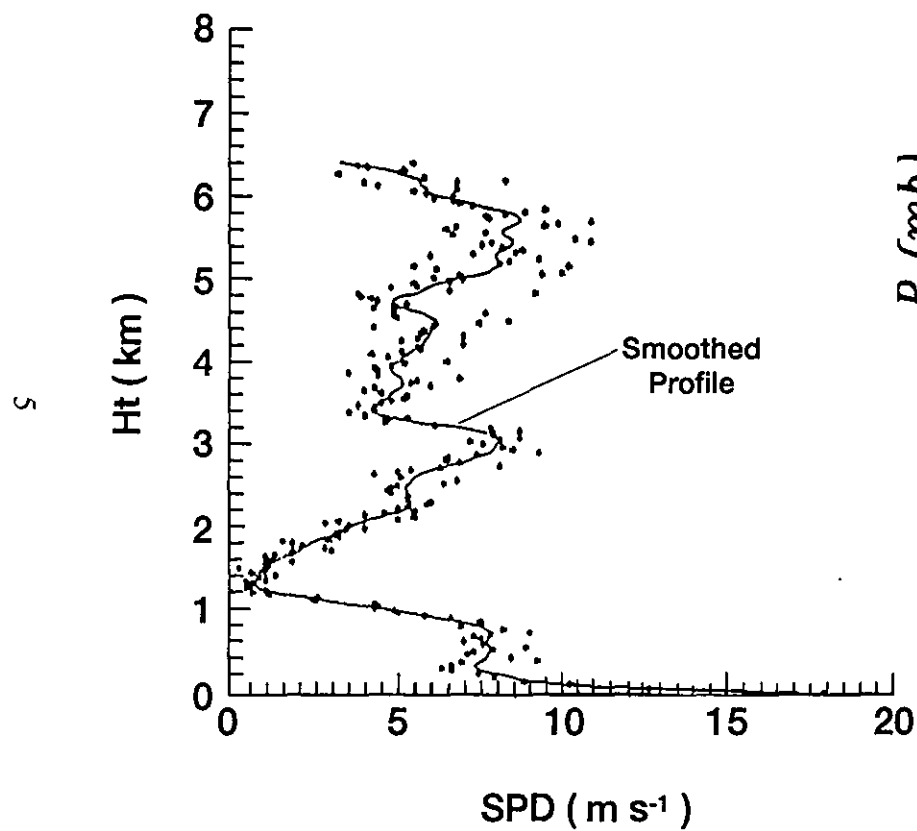


Figure 2. Denver balloon sounding for 2400 UTC on 26 May 1994. The height resolution of the raw data was 34 m. The left panel shows the velocity; the scatter in velocity was smoothed with a 12-point triangular weighting function. The right panel shows dewpoint (left profile) and temperature (right profile).

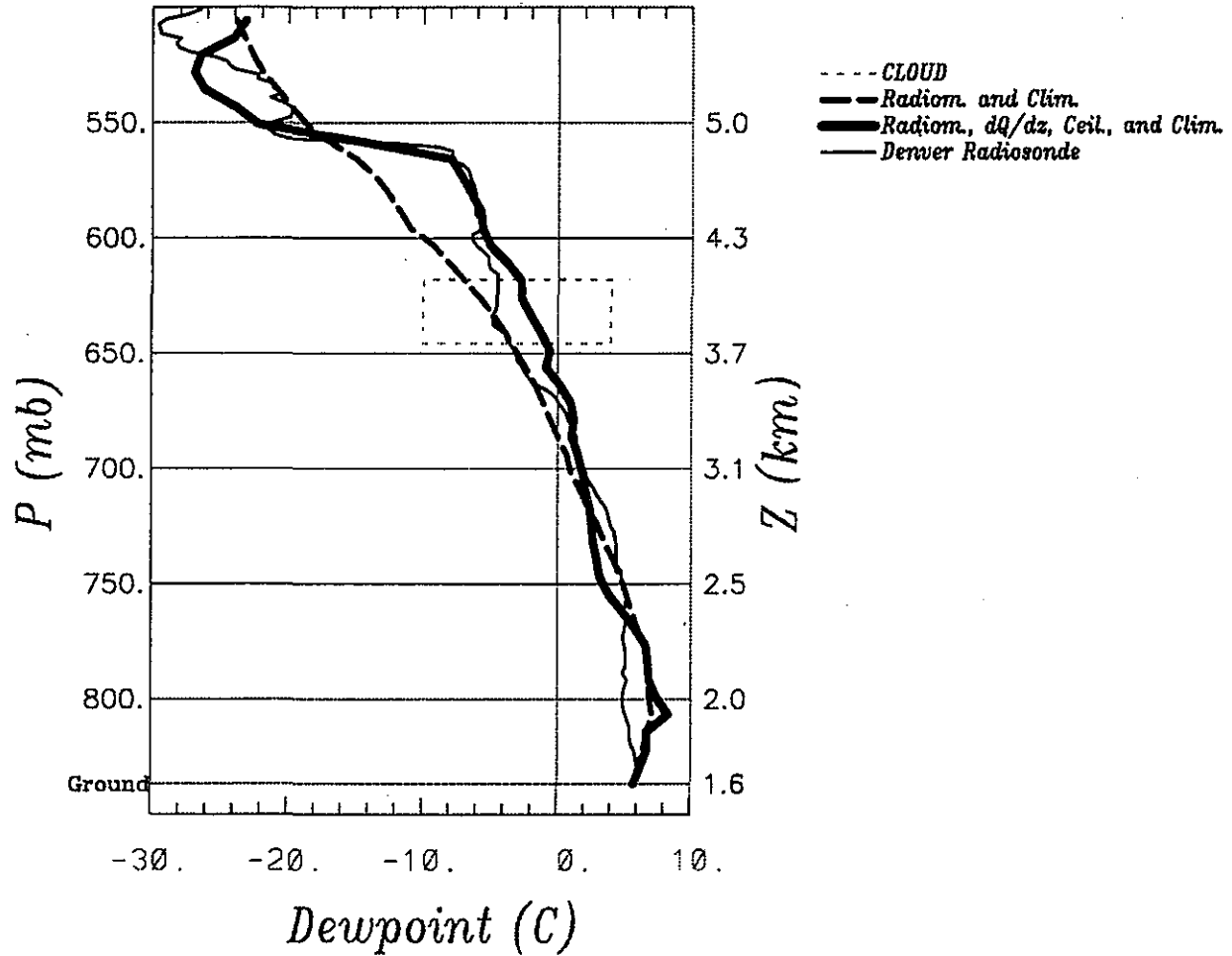


Figure 3. Demonstration of the use of gradient information in the retrieval of details in the humidity profiles provided by microwave radiometers or from Global Positioning Systems (GPS), for 2330 UTC 26 May 1994. The light solid curve is dewpoint from a radiosonde, the heavy dashed curve is the profile that would be given by radiometric retrieval alone, and the heavy solid curve results if the gradient at 560 mb (perhaps provided by radar) is added as a constraint.

spaced sensors. Similar measurements can provide the humidity structure parameter, and the fluctuations of temperature and humidity together yield the refractive index structure parameter. Using a tower at the Boulder Atmospheric Observatory (BAO) at Erie, Colorado (see Kaimal and Gaynor, 1983), we examined relationships (1) and (3). An elevator-mounted carriage was equipped with very-fast-response sensors: platinum wire thermometers, Lyman- α humidity sensors, and sonic anemometers. It was raised and lowered through stratified layers or parked between fixed levels while such layers traversed the tower. The fixed levels were equipped with slow-response, but very accurate, quartz thermometers, dewpointers, and propvane wind sensors. The fast-response sensors were used to measure the structure parameters, and the fixed-level sensors provided accurate height gradients. When the gradients of the means, calculated from the structure functions using (3), were compared with the measured gradients, the results were encouraging (Gossard and Sengupta, 1988), as seen in Fig. 4. The carriage traversed the tower in about 7 minutes. The sensor sampling frequency was 10 Hz. Each time series was 10 s long, so the height resolution was about 7 m and each time series was 100 samples long.

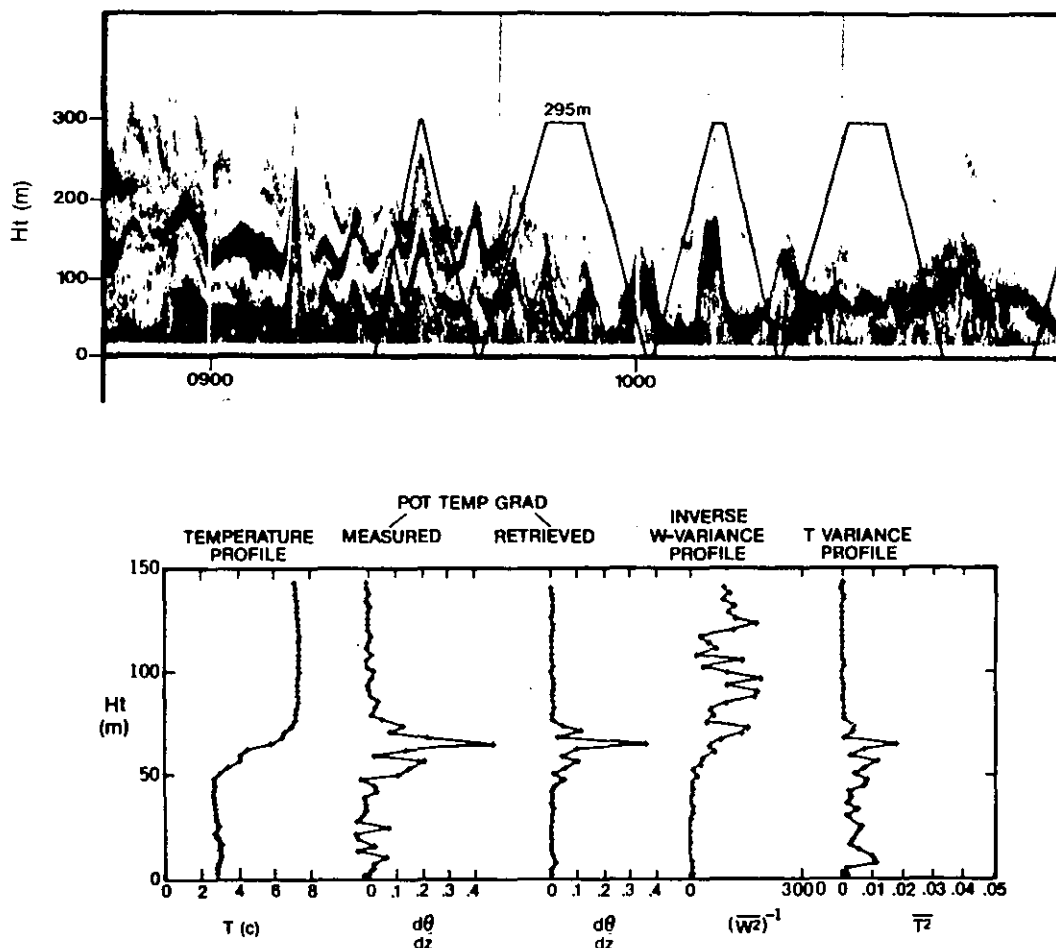


Figure 4. Top frame: Measurements of backscatter from an acoustic sounder, on 29 February 1984, with carriage trajectories (straight-line segments) superimposed. Bottom frame: Measurements of profiles of temperature, potential temperature gradient, vertical velocity variance, and temperature variance, from the carriage. The profiles show the close relationship between the ratio of variances of temperature and w (and therefore of C_θ^2/C_w^2 and the temperature gradient). The sampling period was 0.1 s and each record was 10-s long. Each tower traverse took about 6.5 min, giving a height resolution of about 10 m for the variance profiles. The inverse velocity is shown, so the calculated (retrieved) potential temperature gradient (middle) is proportional to the product of the two right-hand profiles. Compare measured and retrieved potential temperature gradients.

2.2. Radar Observations

Many observational programs have established the validity of the relationship between backscattered power and C_ϕ^2 and some of these results (Kropfli et al., 1968; Bean et al., 1971; Gossard et al., 1984b) are described in the Appendix. The main sources of error in measurements of C_ϕ^2 are due to contamination of the "clear air" backscatter by clouds and insects (Chadwick and Gossard, 1983). Even clouds producing no precipitation at the ground can make a substantial contribution to the radar reflectivity for 915-MHz radars. However, it is anticipated that 404- and 449-MHz wind profiler radars will not be very

vulnerable to clouds except under precipitation conditions, because the reflectivity of small Rayleigh scatterers is inversely proportional to the fourth power of the wavelength. Insects remain an important problem over land, especially in agricultural areas in the warm season, and the lowest kilometer of the atmosphere may not be tractable to radar remote sensing of C_ϕ over land in the summer.

3. C_w^2 PROFILES

3.1. Calculation of C_w^2

The justification for concluding that the Doppler spectral width is a measure of mechanical turbulence intensity depends on the finite size of the pulse volume of the radar. If all scattering elements within the volume were moving toward or away from the radar with the same radial velocity V_r , the backscattered signal would simply be Doppler shifted in frequency by $2V_r/\lambda$, where λ is wavelength, and the spectrum of the signal would have zero width. However, if the scattering elements within the pulse volume are moving with different radial velocities, the spectrum of the backscattered signal will be spread about the mean V_r according to the spread in velocity of the scatterers. For isotropic turbulence, the velocity half-variance is given by

$$\sigma^2 = \int_0^\infty E(k) dk, \quad (7)$$

where, for a fully developed inertial-convective subrange (ICS), the kinetic energy density is

$$E(k) = \alpha \varepsilon^{2/3} k^{-5/3}, \quad (8)$$

$\alpha = 1.6$ is a Kolmogorov constant, and k is wavenumber. Thus, ε is directly related to the total velocity half-variance. However, the radar senses only the variance within the limited pulse volume of the radar. Therefore, observing radial velocity (say w) with a radar whose antenna has finite angular half-beam width α and whose pulse length is ΔR essentially imposes a low-pass filter on the spatial structure of the velocity field being carried past the radar by the wind. Furthermore, if the dwell time t_D of the radar is substantial, the fluctuations are also temporally averaged over t_D , imposing additional low-pass filtering on the fluctuations. Thus a time series of w produced by the Doppler radar contains just low frequencies due to volume averaging and temporal averaging, but lines in the (averaged) Doppler spectra are broadened by the corresponding high-passed frequencies. We use the spectral broadening to calculate turbulent dissipation rate and structure functions, and compare the corresponding spectra with that calculated directly from the time series of $w(t)$. For isotropic, homogeneous turbulence, we note (e.g., Businger, 1982) that

$$\phi_{zz}(k) = \frac{E(k)}{4\pi k^2} \left[1 - \frac{k_z^2}{k^2} \right] \quad (9)$$

for the z component of velocity along the z direction. $E(k)$ is the kinetic energy density spectrum given by (8), and $k^2 = k_x^2 + k_y^2 + k_z^2$. Frisch and Clifford (1974) integrated (9), assuming Gaussian beamwidth and pulse shape (see Gossard and Strauch, 1983, Appendix D) and found [with modifications by Labbitt (1981)]

$$\varepsilon = \frac{1}{\delta} \left[\frac{\sigma_{Vw}^2}{\frac{3}{2}\Gamma\frac{5}{3}\alpha\gamma^2} \right]^{\frac{3}{2}}, \quad (10)$$

where σ_{Vw}^2 is the variance in w within the pulse volume V , and Γ is the gamma function. Here $\alpha \approx 1.6$ is a Kolmogorov constant (see Table 1), and

$$\left. \begin{aligned} \delta &= a \\ h &= 1 - \left[\frac{b}{a} \right]^2 \\ \gamma^2 &= 1 - \frac{h}{15} - \frac{h^2}{105} - \dots \end{aligned} \right\} \text{for } b \leq a ,$$

$$\left. \begin{aligned} \delta &= b \\ h &= 1 - \left[\frac{a}{b} \right]^2 \\ \gamma^2 &= 1 - \frac{4h}{15} - \frac{8h^2}{105} - \dots \end{aligned} \right\} \text{for } b > a ,$$

where a is half the diameter of the (circular) beam cross section and b is the half-length of the pulse. C_w^2 is found from

$$C_w^2 = B_w \varepsilon^{2/3} ,$$

where $B_w = 4/3B$ is another Kolmogorov constant.

3.2. Experimental Comparison of C_w^2 Retrievals With Measured Spectra

Early efforts to compare C_w^2 values measured by sonic anemometers mounted on a tower, with radar-measured values from spectral second moments were unsatisfactory (Gossard et al., 1984a), mainly because the proximity of the tower led to very large, spurious returns through the side-lobes of the antenna unless the radar was moved so far from the tower that comparison of the measurements was not very useful. In the present experiment, it was decided to compare the spectrum of the time series of radial (vertical) velocity with the corresponding spectrum implied by the Doppler spectral width. Twenty-minute time series of w from range gates 2–6 and gate 19 (at a frontal interface) are shown in Fig. 5. The data were collected with a 449-MHz wind profiler whose characteristics are shown in Table 2.

The derivation of the relationship between spectral width and structure parameter assumes the inertial subrange exists out to scales comparable with the pulse volume size. (From Table 2, note that the height spacing is 180 m, and from two-way beamwidth in degrees, the width of the beam is about 135 m at a height of 1 km.) Then the spectrum of the velocity perturbations is given by

$$S_w(k) = 0.249 C_w^2 k^{-5/3} , \quad (11)$$

where k is the spatial wavenumber of the turbulence and it is assumed that $k = 2\pi f/u_0$ (Taylor's

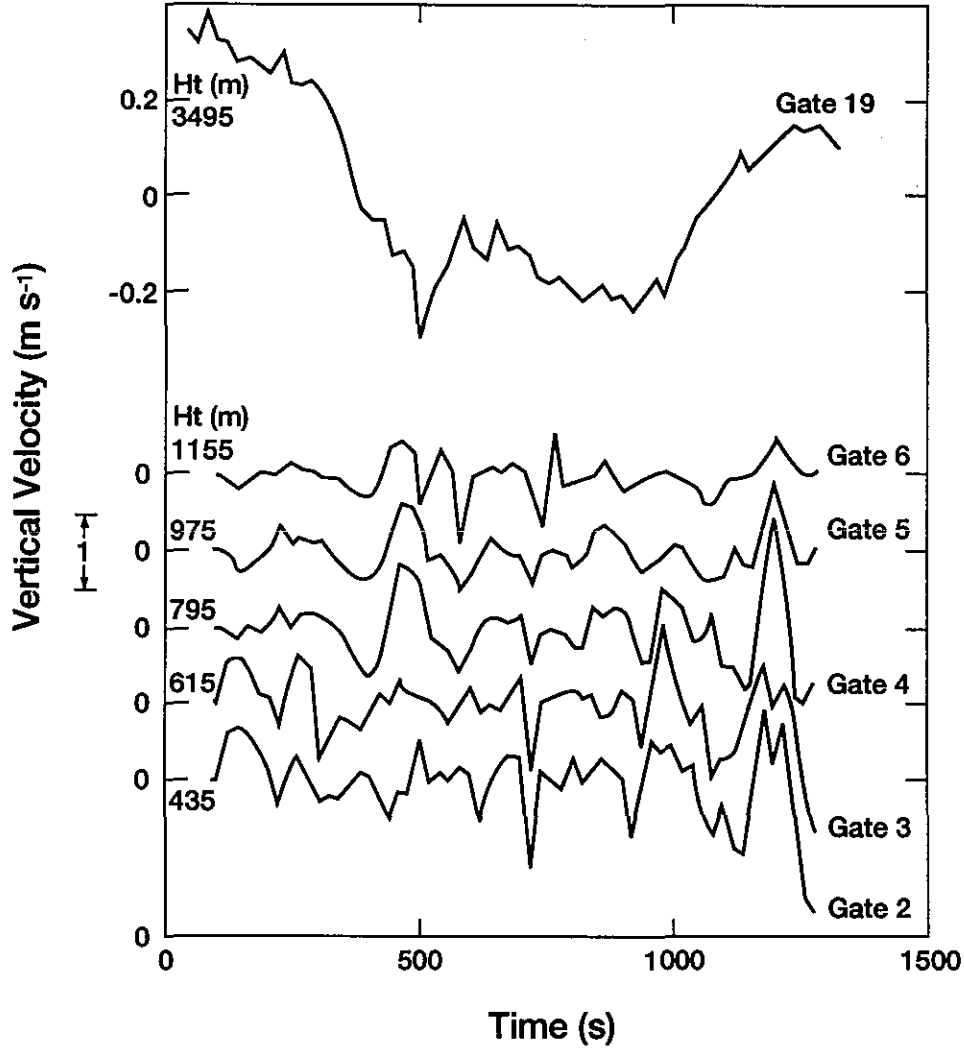


Figure 5. Twenty-minute (64-point) time series of vertical velocity for selected range gates. The sampling interval is 19 s. The time series were spectrum analyzed by a fast Fourier transform (FFT) for subsequent comparison with spectra deduced from the width of the radar Doppler velocity spectra. Thus the spatial sampling interval, assuming a 5 m s^{-1} wind, was about 95 m.

hypothesis), where f is frequency in hertz. This spectrum can be compared directly with the spectrum derived from the time series of w , which extends out to the Nyquist frequency f_n corresponding to a scale of

$$L_n = \frac{u_0}{f_n}, \quad (12)$$

which is about 200 m at a wind speed of 5 m s^{-1} for our sampling rate (20-s sampling interval). Figure 6 shows spectra from the 20-min time series in Fig. 5 using a 64-point fast Fourier transform (FFT) with a log-log regression fit superimposed (solid). The corresponding spectra deduced from C_w^2 , found from the mean Doppler spectral width using (10), is also shown (dashed) for comparison. The agreement is convincing, and the radar-measured values of turbulent intensity (C_w^2) are apparently comparable with the accuracy of C_ϕ^2 deduced from backscattered power; however, more experiments are needed.

Table 2. Characteristics of the 449-MHz wind profiler radar.

Characteristics	Value
Frequency	449 MHz
Bandwidth	1 MHz
Peak power	900 W
Antenna aperture	4.25×4.25 m
Two-way beamwidth	5.7°
Pulse width	1.2 μ s
Gate spacing	1.2 μ s
Pulse repetition period	60 μ s
No. pulses averaged	220
No. spectra averaged	10
Folding velocity	12.6 m s ⁻¹
Spectral resolution	0.2 m s ⁻¹
First height	255 m
Height spacing	180 m
Number of heights	32

3.3. Turbulence Profile Retrieval on 26 May 1994

During the period when the data were collected to test the accuracy of radar-measured C_w^2 , a stationary front existed over the eastern slope (Front Range) of the Rocky Mountains, producing a strong humidity gradient at a height of about 3.5 km. In this area it is usual for such a frontal interface to be accompanied by clouds that contaminate the C_ϕ^2 measurement. However, at the time of the radar observations there were no clouds at the Erie site. The nearest balloon sounding available for in situ comparison was the Denver sounding taken at about 2300 UTC, 60 km from the radar site at Erie. However, because the front was fairly stationary and horizontally uniform, it was decided to compare it with the radar retrieval in spite of the spatial and temporal separation. In this test the radar was pointing vertically, so no profile of horizontal wind was obtained. Because the horizontal wind can be important in artificially broadening the spectrum if the radar beamwidth is not zero (beamwidth = 5° for this radar), a small correction was made assuming a 5 m s⁻¹ wind based on the Denver wind sounding.

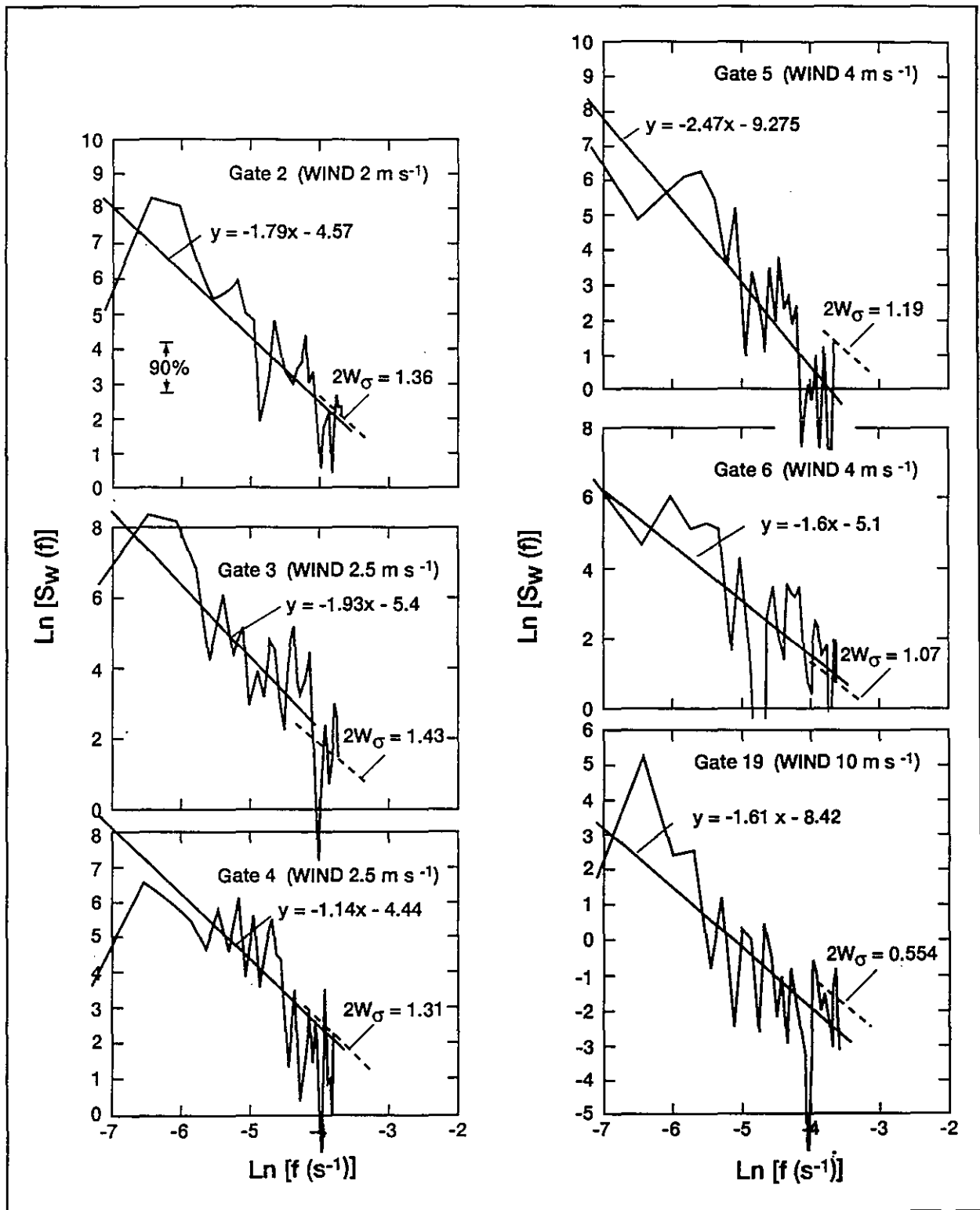


Figure 6. Spectra from the time series shown in Fig. 5. The solid straight lines are log-log linear regression fits of spectral density and frequency. The dashed linear segments are spectra plotted from the C_w^2 found from the radar Doppler spectral width $2w_\sigma$.

The balloon profiles are shown in Fig. 2. Nine radar-measured C_ϕ^2 profiles from the beginning of the observation period are shown in Fig. 7a and eight from the end are shown in Fig. 7b to demonstrate the persistency of the main features. In Fig. 8 the corresponding profiles of C_w^2 are shown, and in Fig. 9 the mean profiles are shown.

Figure 10 shows the mean profile of turbulent dissipation rate ϵ together with mean C_w^2 , for the beginning of the period, and Fig. 11 shows the corresponding height distribution of the outer scale L_0 and the Kolmogorov microscale η , where

$$L_0 = \left[\frac{C_w^2}{(du/dz)^2} \right]^{3/4} \quad (13a)$$

and

$$\eta = \left[\frac{v^3}{\epsilon} \right]^{1/4}, \quad (13b)$$

and v is kinematic viscosity (Gossard et al., 1984).

4. REFRACTIVE INDEX AND HUMIDITY PROFILE RETRIEVAL ON 26 MAY 1994

There are clearly two main features of the C_ϕ^2 profiles (Fig. 7): a strong peak between 0.3 and 1 km and another major peak at the frontal interface at about 3.5 km. The mean profiles of C_ϕ^2 and C_w^2 were used in Eq. (3). The radar did not measure wind profiles or RASS output in this experiment, so it was necessary to use winds from the Denver balloon sounding for the shear factor and for temperature in the humidity retrieval (see Appendix, Sec. A.3). The resulting retrieved profiles (solid) of the gradients of potential refractive index (i.e., ϕ) are shown in Fig. 12 for the first period (left) and for the second period (right). The humidity gradient profile is shown in Fig. 13. The radar retrievals apparently underestimate the balloon-measured gradients. However, if the height of the gradient of C_ϕ^2 in the Denver sounding is compared with the height of the peak in C_ϕ^2 measured by the radar at Erie, it is seen that the peak in C_ϕ^2 is 100–200 m higher. If the radar sounding is shifted down by one range gate (180 m), the resulting retrieval is improved but still underestimates the balloon-measured gradient by roughly a factor of 2. Considering the poor resolution of the radar and the separation of the radar and balloon observations in space and time, the agreement between the two is considered encouraging.

The reason for the large peak in C_ϕ^2 below 1 km remains uncertain. There is no obvious meteorological mechanism for producing such large backscatter in a well-mixed boundary layer where there are no large gradients of mean properties. It is our tentative conclusion that the scatterers are insects, because it is well established (Chadwick et al., 1976; McLaughlin, 1994) that the convective boundary layer contains a multitude of insects at this time of year in the midwest United States. Clearly it would be useful to conduct an experiment in which two or more radar wavelengths were used to identify particulate scatterers.

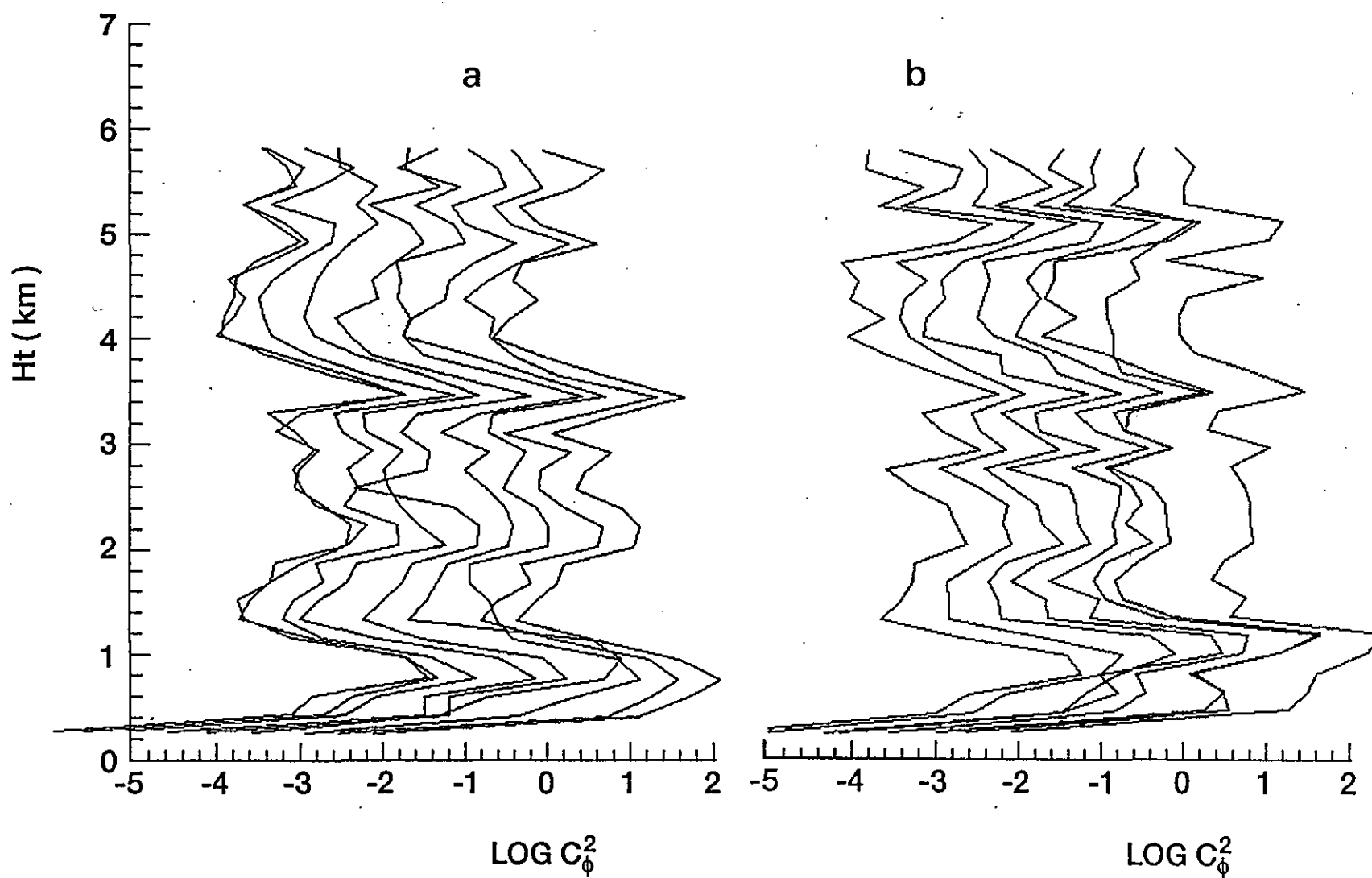


Figure 7. (a) Nine side-by-side radar-measured profiles of $C_{\phi}^2 = C_N^2$ (see the Appendix) at the beginning of the 20-min period, and (b) eight at the end of the period, at Erie on 26 May 1994. Note the strong layer at the height of the front and in the lowest kilometer. Profiles are separated by 19 s in time. The scale applies to the left-most profile.

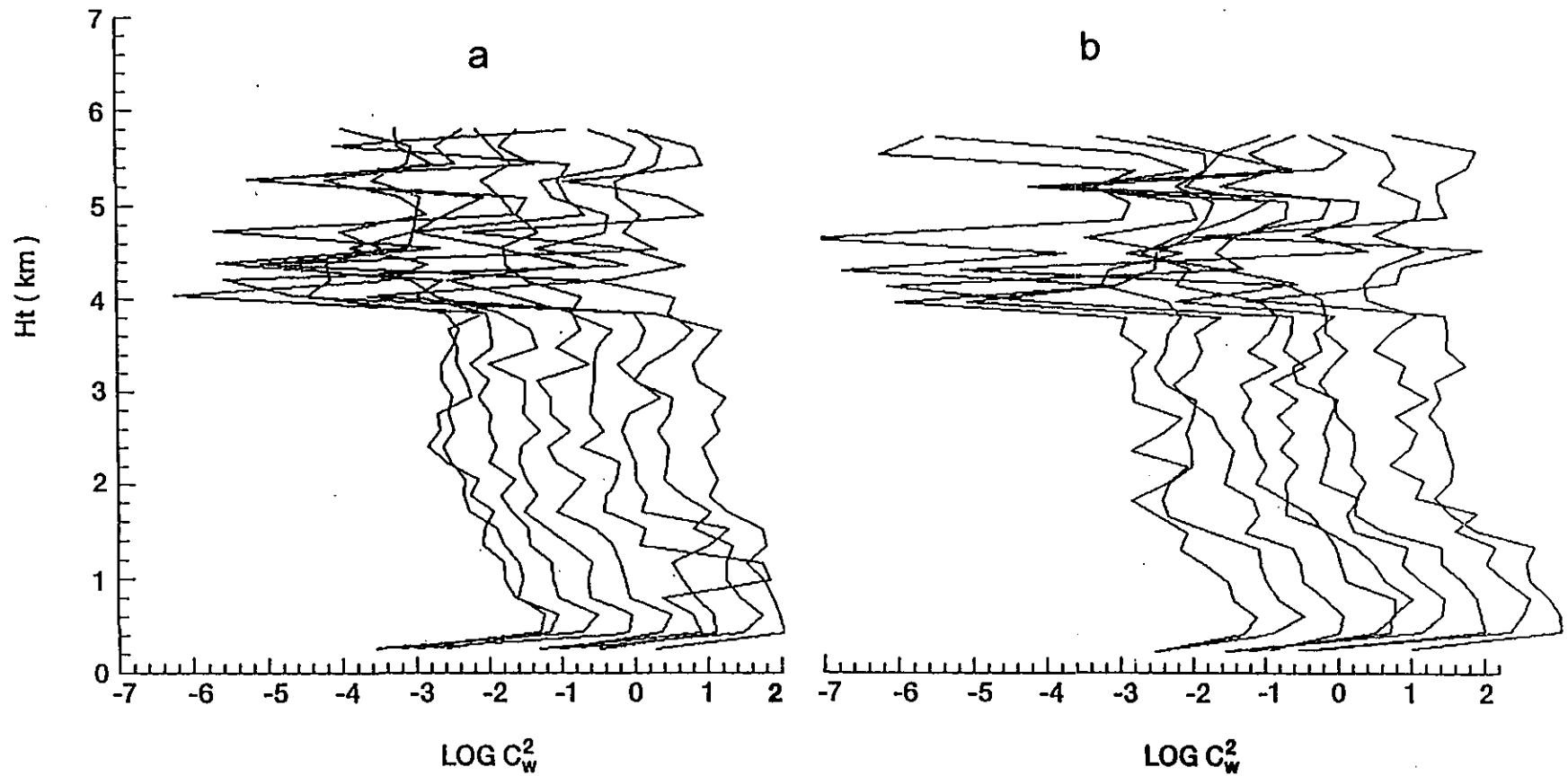


Figure 8. (a) Nine side-by-side radar-measured profiles of C_w^2 at the beginning of the 20-min period, and (b) eight at the end of the period, at Erie on 26 May 1994. Note the noisy character of the C_w^2 profiles above the front where the signal falls off sharply. The scale applies to the left-most profile.

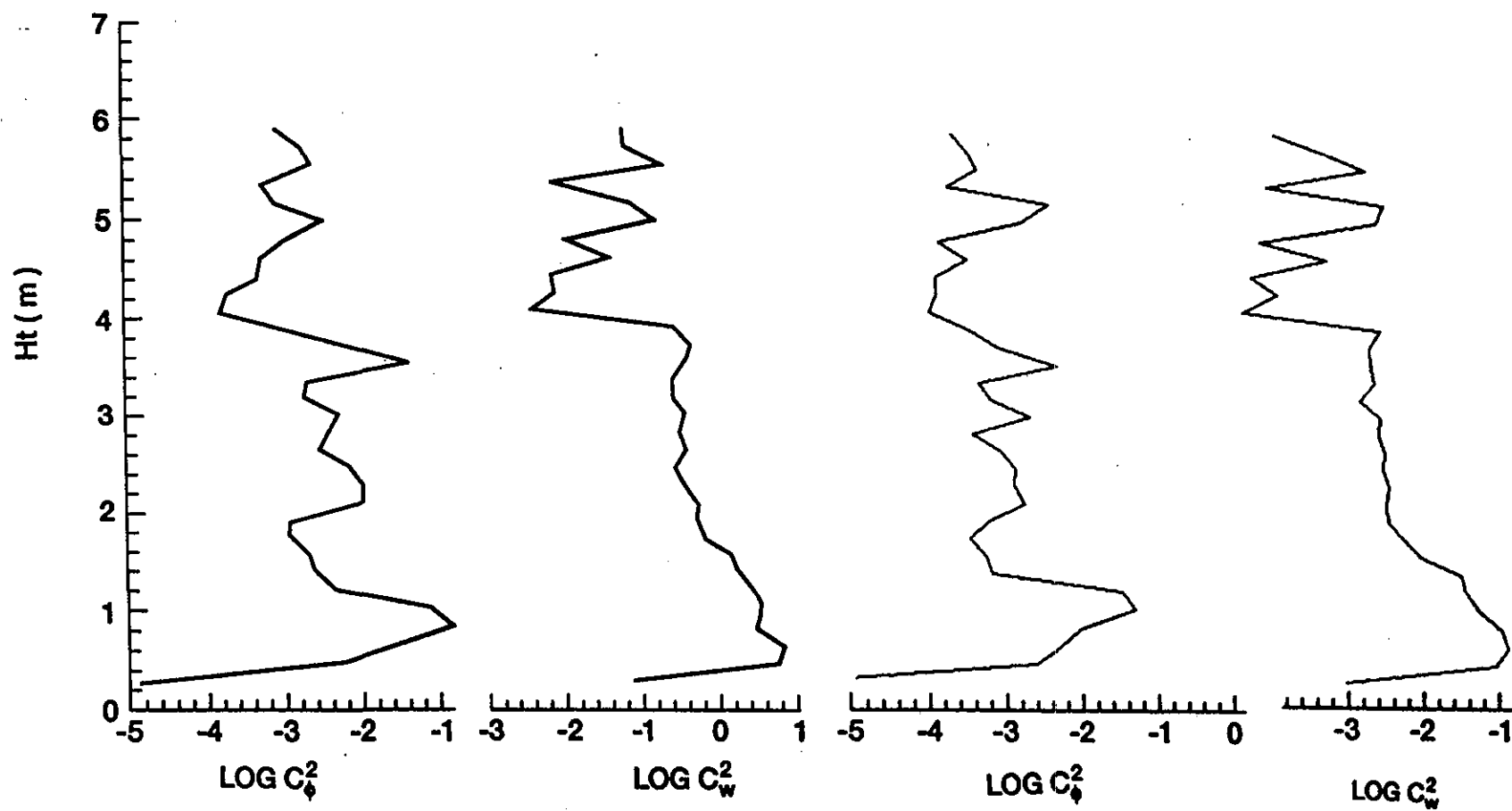


Figure 9. Average log of C_ϕ^2 and log C_w^2 for 12 profiles from 1700-1704 UTC (left) and 1716-1720 UTC (right), 26 May 1994.

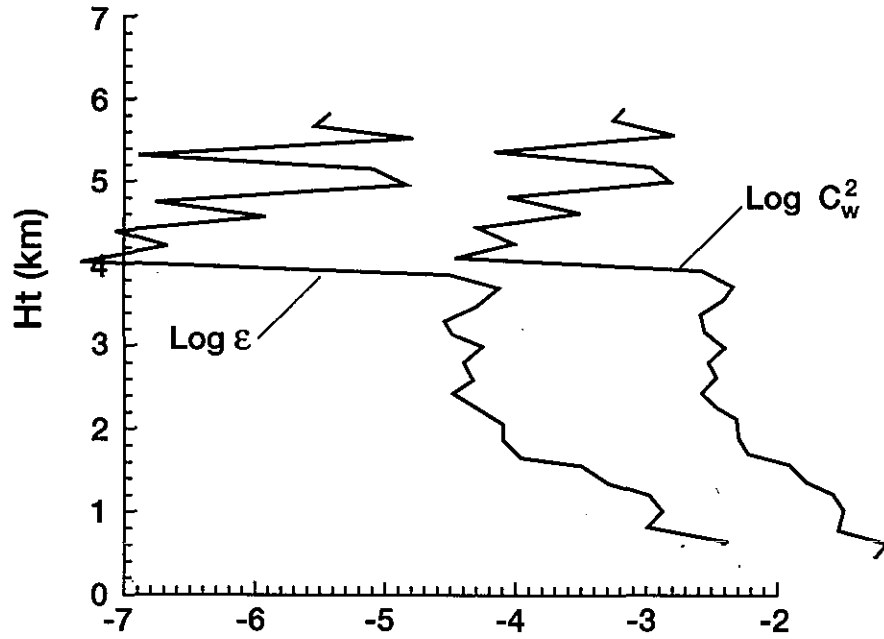


Figure 10. Average of $\log \varepsilon$ for the average of the C_w^2 profiles in Fig. 8a; ε is turbulent dissipation rate ($\text{m}^2 \text{s}^{-3}$).

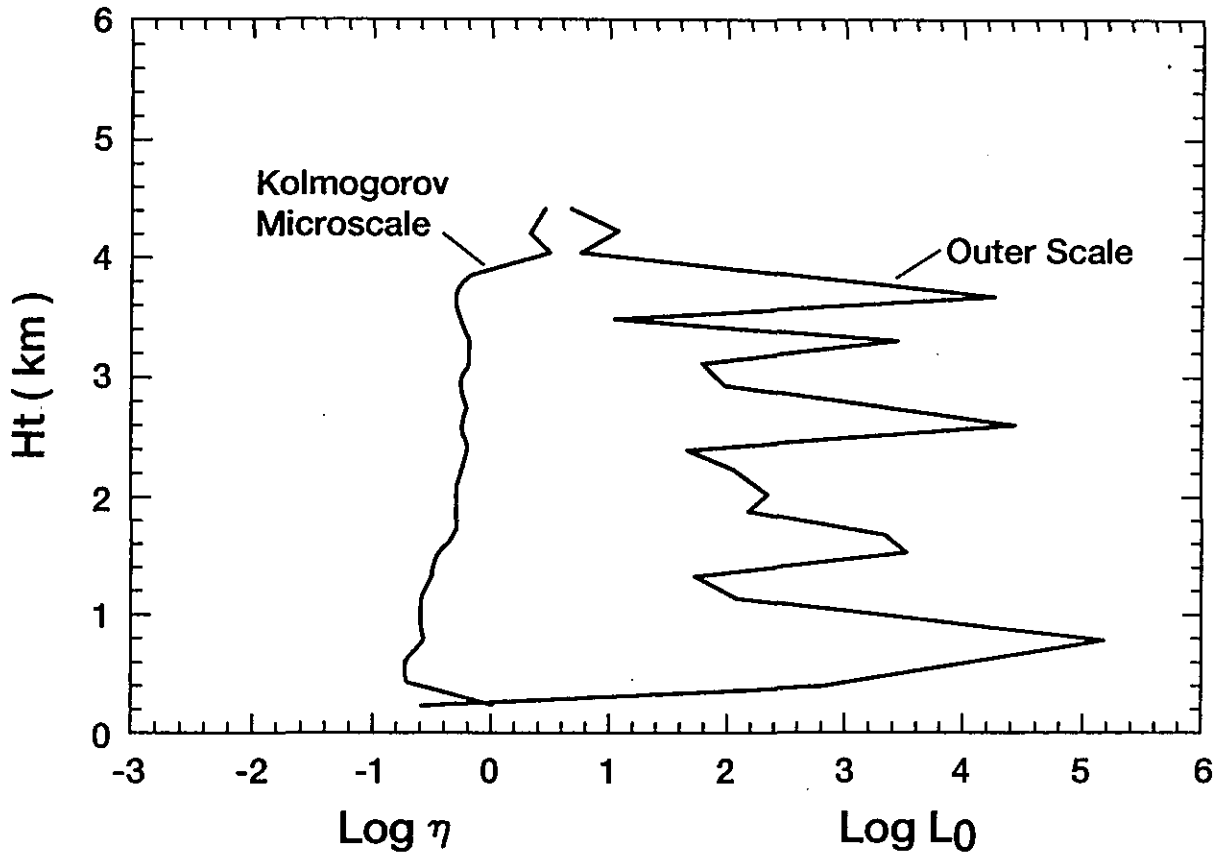


Figure 11. Average of $\log \eta$ and L_0 for the same profiles as in Fig. 10; L_0 is turbulent outer scale (m) and η is the Kolmogorov microscale.

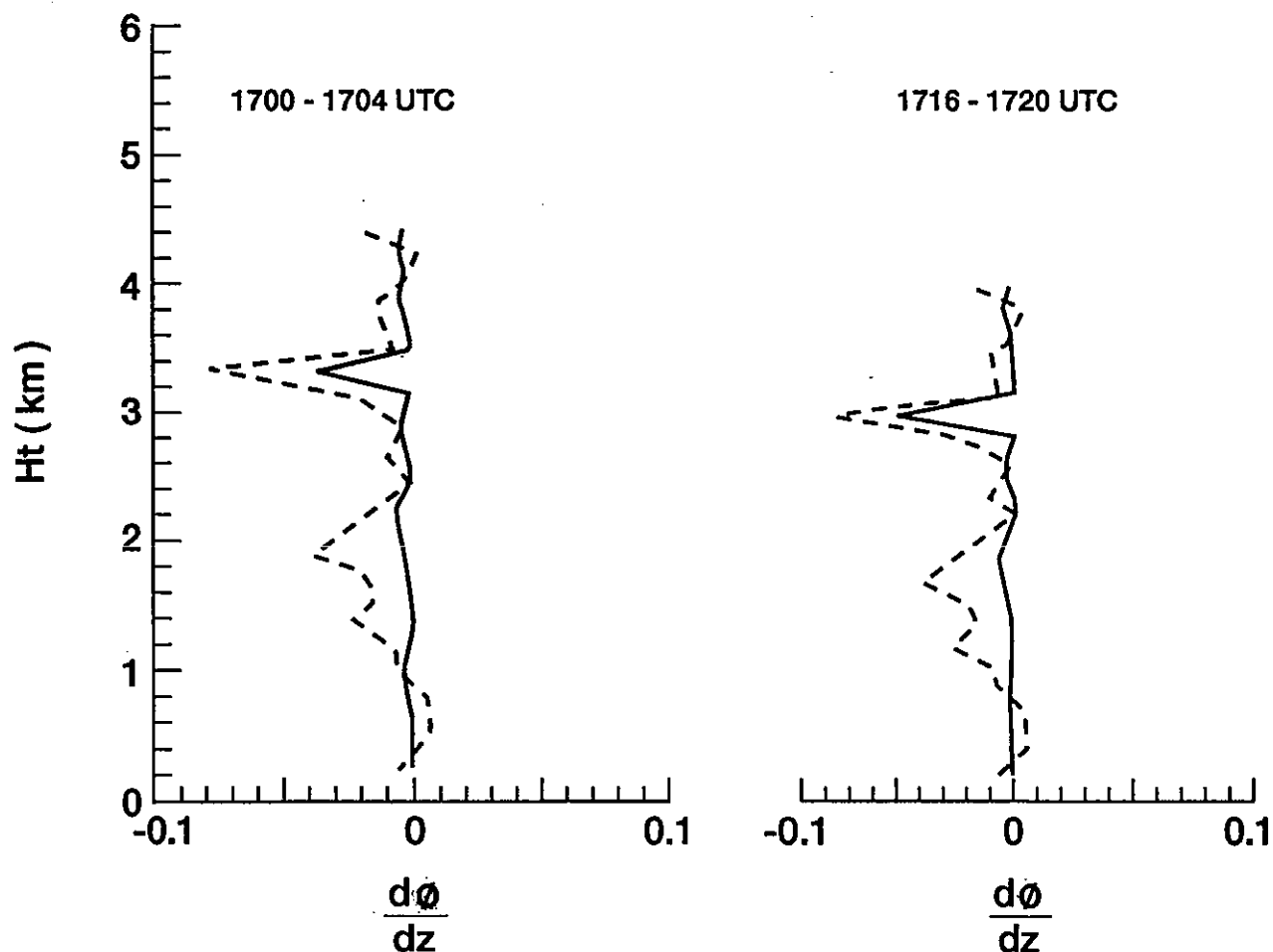


Figure 12. Profile of height gradients of potential refractive index [Eq. (A8)]: balloon-measured (dashed) and calculated from profiles in Fig. 9 using Eq. (3) (solid). The peak at 3.3 km is the frontal interface.

5. CONCLUSIONS

The experiment described in this paper lends support to the accuracy of the radar technique that uses the width of the Doppler spectrum of refractive index turbulent backscatter to remotely sense the intensity of mechanical turbulence. It provides profiles of turbulent intensity, turbulence outer scale, and velocity structure parameter. Together with wind shear and the profile of C_n^2 , it can be used to calculate gradients of refractive index aloft, and, with RASS, to deduce humidity gradients. However, the accuracy of these calculations remains to be determined by further observation, because they use all the observational capability of the profilers, i.e. the zero, first, and second moments of the Doppler spectra and the RASS temperatures.

6. REFERENCES

Andreas, E.L., 1987: On the Kolmogorov constants for the temperature-humidity cospectrum and the refractive index spectrum. *J. Atmos. Sci.*, **44**, 2399–2406.

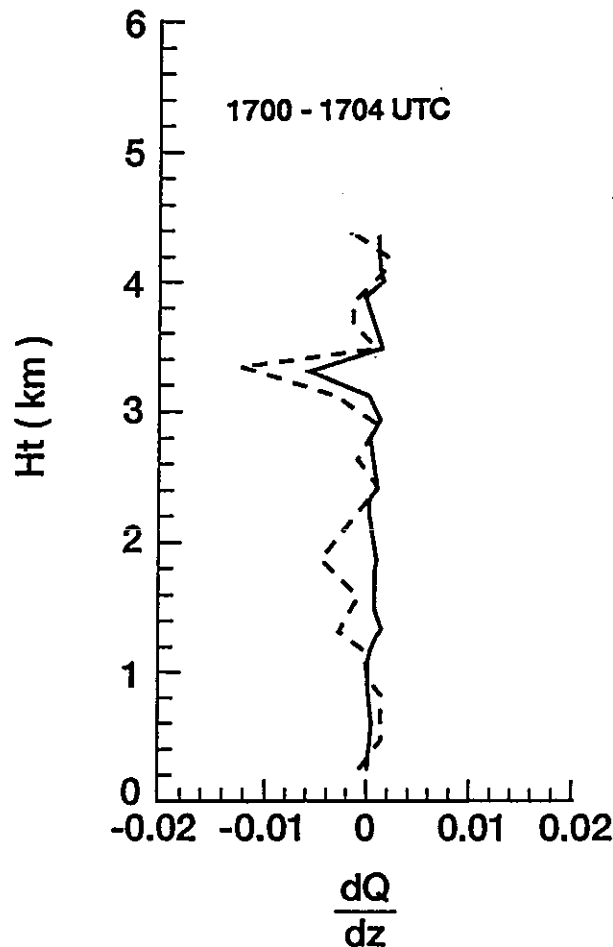


Figure 13. Profile of height gradients of specific humidity (g kg^{-1}), 26 May 1994: balloon-measured (dashed) and calculated from Eq. (A11) (solid). The temperature gradients used in calculating the humidity gradients were taken from the balloon, because no RASS soundings were available.

- Atlas, D., 1964: Advances in radar meteorology. *Adv. Geophys.*, **10**, 317–478.
- Atlas, D., K. Hardy, K.M. Glover, I. Katz, and T.G. Konrad, 1966: Tropopause detected by radar. *Science*, **153**, 1110–1112.
- Battán, L.J., 1973: *Radar Observation of the Atmosphere*. University of Chicago Press, Chicago, 323 pp.
- Bean, B.R., and E.J. Dutton, 1966: *Radio Meteorology*. Monogr. 92, National Bureau of Standards, Gaithersburg, MD, 435 pp.
- Bean, B.R., R.E. McGavin, R.B. Chadwick, and B.B. Warner, 1971: Preliminary results of utilizing the high resolution FM radar as a boundary layer probe. *Bound.-Layer Meteor.*, **1**, 466–473.
- Businger, J.A., 1982: Equations and concepts. In *Atmospheric Turbulence and Air Pollution Modelling*, F.T.M. Nieuwstadt and H. van Dop (eds.), Reidel, Hingham, MA, 1–39.
- Chadwick, R.B., and E.E. Gossard, 1983: Radar remote sensing of the clear atmosphere—Review and applications. *Proc. IEEE*, **71**, 738–753.

- Chadwick, R.B., K.P. Moran, R.G. Strauch, and G. Morrison, 1976: Microwave radar wind measurements in the clear air. *Radio Sci.*, **11**, 795–802.
- Doviak, R.J., and D.S. Zrnić, 1984: *Doppler Radar and Weather Observations*. Academic, San Diego, CA, 458 pp.
- Friehe, C.A., J.C. LaRue, F.H. Champagne, C.H. Gibson, and G.F. Dreyer, 1975: Effects of temperature and humidity fluctuations on the optical refractive index in the marine boundary layer. *J. Opt. Soc. Am.*, **65**, 1502–1511.
- Frisch, A.S., and S.F. Clifford, 1974: A study of convection capped by a stable layer using Doppler radar and acoustic echo sounders. *J. Atmos. Sci.*, **31**, 1622–1628.
- Gage, K.S., J.L. Green, and T.E. VanZandt, 1980: Use of Doppler radar for the observation of atmospheric turbulence parameters from the intensity of clear air echoes. *Radio Sci.*, **15**, 407–416.
- Gorelik, A.G., and Y.V. Mel'nychuk, 1963: Radar study of dynamic processes in the atmosphere. *Tr. Vses. Nav. Meteor. Souesh.*, No. 5.
- Gossard, E.E., 1960: Power spectra of temperature, humidity, and refractive index from aircraft and tethered balloon measurements. *IRE Trans. Antennas Propag.*, **AP-8**, 186–201.
- Gossard, E.E., and R.G. Strauch, 1983: *Radar Observations of Clear Air and Clouds*. Elsevier, New York, 280 pp.
- Gossard, E.E., and N. Sengupta, 1988: Measuring gradients of meteorological properties in elevated layers with a surface-based Doppler radar. *Radio Sci.*, **23**, 625–693.
- Gossard, E.E., R.B. Chadwick, W.D. Neff, and K.P. Moran, 1982: The use of ground-based Doppler radars to measure gradients, fluxes and structure parameters in elevated layers. *J. Appl. Meteor.*, **21**, 211–226.
- Gossard, E.E., R.B. Chadwick, R.T. Detman, and J. Gaynor, 1984a: Capability of surface-based, clear-air Doppler radar for monitoring meteorological structure of elevated layers. *J. Clim. Appl. Meteor.*, **23**, 474–490.
- Gossard, E.E., W.D. Neff, R.J. Zamora, and J.E. Gaynor, 1984b: The fine structure of elevated refractive layers: Implications for over-the-horizon propagation and radar sounding systems. *Radio Sci.*, **19**, 1523–1533.
- Gurvich, A.S., 1968: Effect of absorption on the fluctuation in signal level during atmospheric propagation. *Radio Eng. Electron. Phys.* (English Transl.), **13**, 1687–1694.
- Hill, R.J. 1978: Models of the scalar spectrum for turbulent advection. *J. Fluid Mech.*, **88**, 541–562.
- Hill, R.J., 1989: The structure functions and spectra of scalar quantities in the inertial convective and viscous convective ranges of turbulence. *J. Atmos. Sci.*, **46**, 2245–2251.
- Hocking, W.K., 1983: On the extraction of atmospheric turbulence parameters from radar backscatter Doppler spectra: I, Theory. *J. Atmos. Terr. Phys.*, **45**, 89–102.
- Kaimal, J.C., and J.E. Gaynor, 1983: The Boulder Atmospheric Observatory. *J. Appl. Meteor.*, **22**, 863–880.
- Kondo, J., O. Kanechika, and N. Yasuda, 1978: Heat and momentum transfers under strong stability in the atmospheric turbulent layer. *J. Atmos. Sci.*, **35**, 1012–1021.

- Kropfli, R.A., I. Katz, T.G. Konrad, and E.B. Dobson, 1968: Simultaneous radar reflectivity measurements and refractive index spectra in the clear atmosphere. *Radio Sci.*, **3**, 991–994.
- Labbitt, M., 1981: Coordinated radar and aircraft observations of turbulence. *Rep. ATC-108*, MIT Lincoln Laboratory, Cambridge, MA, 40 pp.
- McLaughlin, S.A., 1994: FM-CW observations of insects and birds in the planetary boundary layer at White Sands Missile Range, New Mexico. *Proc., 11th Conf. on Biometeorology and Aerobiology*, American Meteorological Society, Boston, MA, 419–422.
- Ottersten, H., 1969: Atmospheric structure and radar backscattering in clear air. *Radio Sci.*, **4**, 1179–1193.
- Priestley, J.T., and R.J. Hill, 1985: Measuring high-frequency humidity, temperature, and radio refractive index in the surface layer. *J. Atmos. Oceanic Technol.*, **2**, 233–251.
- Richter, J.H., 1969: High-resolution tropospheric radar sounding. *Radio Sci.*, **4**, 1260–1268.
- Srivastava, R.C., and S.D. Atlas, 1972: The effects of a finite radar pulse volume on turbulence measurements. *Preprints, 15th Radar Meteorology Conf.*, American Meteorological Society, Boston, MA, 297–302.
- Stankov, B.B., E.R. Westwater, and E.E. Gossard, 1995: High vertical resolution humidity profiling from combined remote sensors. *J. Atmos. Oceanic Technol.* (submitted).
- Strauch, R.G., and F.H. Merrem, 1976: Structure of an evolving hailstorm: III, Internal structure from Doppler radar. *Mon. Weather Rev.*, **104**, 588–595.
- Strauch, R.G., D.A. Merritt, K.P. Moran, K.B. Earnshaw, and D. van de Kamp, 1984: The Colorado wind-profiling network. *J. Atmos. Oceanic Technol.*, **1**, 37–49.
- Tatarskii, V.I., 1971: The effects of the turbulent atmosphere on wave propagation. Israel Program for Scientific Translations, Jerusalem, 472 pp. [NTIS TT-68-50464].
- VanZandt, T.E., J.L. Green, K.S. Gage, and W.L. Clark, 1978: Vertical profiles of refractivity turbulence structure constant: Comparison of observations by the Sunset radar with a new theoretical model. *Radio Sci.*, **13**, 819–829.
- Warnock, J.M., and T.E. VanZandt, 1985: A statistical model to estimate the refractivity turbulence structure constant C_n^2 in the free atmosphere. *NOAA TM ERL AL-10*, NOAA Environmental Research Laboratories, Boulder, CO, 175 pp.
- Wyngaard, J.C., W.T. Pennell, D.H. Lenshaw, and M.A. LeMone, 1978: The temperature-humidity covariance budget in the convective boundary layer. *J. Atmos. Sci.*, **35**, 48–58.

Appendix

A.1. INTRODUCTION

Radar measurement of C_n^2 for atmospheric backscatter is described in many standard texts [e.g., Atlas, 1964; Battan, 1973; Gossard and Strauch, 1983, Eq. (15Aa); Doviak and Zrnić, 1984, Eq. (4.25)]. Many publications illustrate the detail with which backscattered power reveals the refractive index turbulence (RIT) structure of the clear atmosphere (e.g., Richter, 1969). For the present purposes we neglect attenuation in the intervening medium between scatterer and radar and consider only backscatter. Then, designating A_e as the effective area of the antenna and η as the radar reflectivity,

$$P_r \propto P_t A_e \frac{\Delta r}{r^2} \eta, \quad (\text{A1})$$

where P_r and P_t are power received and transmitted, Δr is the range resolution (equal to $c\tau/2$, where τ is pulse duration), and r is the range to the target. The proportionality factor in (A1) is a constant that depends on assumptions about the antenna beam (often chosen to be either "top hat" or Gaussian). Depending on the definition of P_r , it may (e.g., Doviak and Zrnić, 1984) incorporate properties of the receiver, such as bandwidth.

For an arbitrary scattering angle α (the angle between the incident and the scattering directions), η is given by [e.g., Doviak and Zrnić, 1984, Eq. (11.93); Gossard and Strauch, 1983, Eq. (2-41)]

$$\eta = 2\pi k_r^4 \frac{E_n(\kappa)}{\kappa^2} \sin^2 \chi, \quad (\text{A2})$$

where $k_r = 2\pi/\lambda$ and λ is wavelength, $\kappa = 2k_r \sin(\alpha/2)$, $E_n(\kappa)$ is the power spectrum of the refractive index (n) fluctuations, and $E_n(\kappa) = -\kappa[\partial S(\kappa)/\partial \kappa]$ where $S(\kappa)$ is the one-dimensional spectrum along a line through a medium whose turbulence is isotropic and homogeneous. Thus, the important scattering scale in the medium is $2\pi/\kappa$, often called the Bragg scale. In the radar equation [(A1)] we are, of course, considering only backscatter. Then $\alpha = \pi$ so that $\kappa = 2(2\pi/\lambda)$, and the Bragg scale is $\lambda/2$. It is therefore clear that radars remotely sense the refractive index variance density of the spectral component corresponding to half the radar wavelength, and it is useful to examine whether useful meteorological information can be extracted from radar measurements of backscattered power using (A1) and (A2). For example, it has often been assumed that the refractive index spectrum in the neighborhood of the Bragg scale has the inertial-convective subrange (ICS) form so that the radar refractive index spectrum follows the same $\kappa^{-5/3}$ law that governs potential temperature and specific humidity; a great deal of work has gone into examining the rigor of this assumption (e.g., Hill, 1978). Assuming the ICS form for the spectra,

$$\begin{aligned} S_u(k) &= 0.249 C_u^2 k^{-5/3}, \\ S_\theta(k) &= 0.249 C_\theta^2 k^{-5/3}, \\ S_n(k) &= 0.249 C_n^2 k^{-5/3}, \end{aligned} \quad (\text{A3})$$

which can be considered to define the structure parameters (Ottersten, 1969) for the (say) z component of velocity (C_w^2), temperature (C_θ^2), and refractive index (C_n^2); k is the wavenumber along a line through

the turbulent fluid. If the refractive index spectrum takes the ICS form, the radar reflectivity for RIT backscatter is as given by Atlas et al. (1966) and Ottersten (1969),

$$\eta \approx 0.38 C_n^2 \lambda^{-1/3}, \quad (\text{A4a})$$

compared with

$$\eta \approx \frac{\pi}{16} |K|^2 k_r^4 Z \quad (\text{A4b})$$

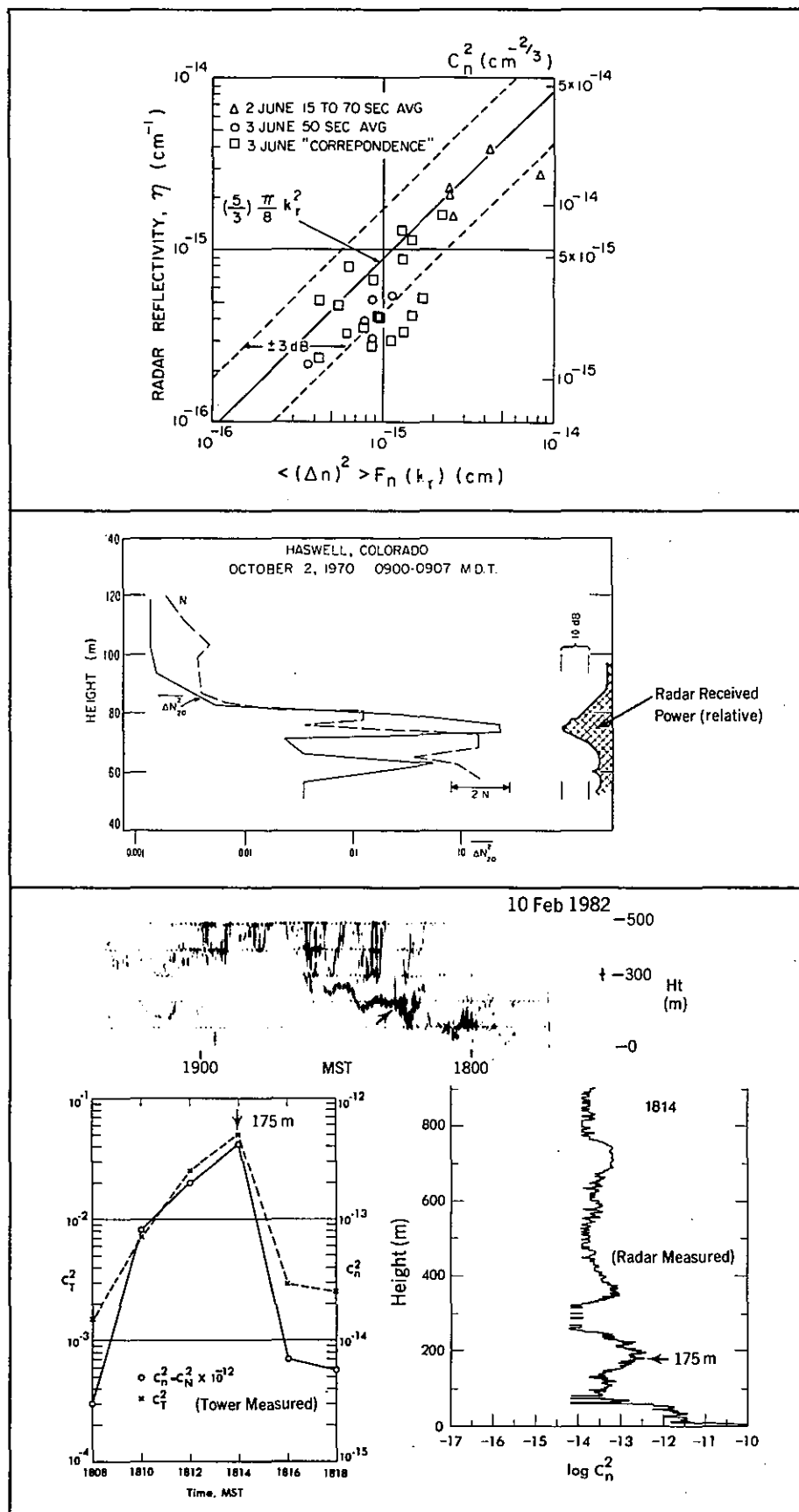
for the reflectivity from spherical Rayleigh particulates, where $|K|^2 \approx 0.93$ for liquid water and Z is the radar reflectivity factor.

A more fundamental definition of the structure parameter is $\overline{[n(r) - n(r+l)]^2} = C_n^2 l^{2/3}$, where r is the position of measurement in the fluid, l is sensor separation, and n is refractive index defined in terms of ϕ (Sec. A.2). The overbar indicates a spatial average. A measurement of the variance at a given l is a measure of C_n^2 [and therefore of η from (A4) in the ICS]. Several experiments combining radar and in situ sensors have established the validity of these relationships. Three are summarized in Fig. A1. The top frame, from Kropfli et al. (1968), shows observed radar reflectivity η versus spectral power of refractive index fluctuations at the radar half-wavelength of 5.35 cm. Spectral power was obtained by extrapolating computed spectra (based on airborne microwave refractometer measurements) down to wavenumber k_r , at the Bragg scale. We see that for almost all cases the radar reflectivity corresponds within 3 dB to that expected from direct refractometer measurements for Bragg scatter in the ICS.

The middle frame shows a similar comparison reported by Bean et al. (1971). In this experiment $\Delta N_{20}^2 = [N(r) - N(r+0.2)]^2$, where $N = (n-1) \times 10^6$ [Eq. (A6)] was measured with a microwave refractometer having two cavities separated by 0.2 m (20 cm) as it traversed a 150-m tower near Haswell, Colorado. The radar backscattered power was measured with a vertically pointing FM-CW radar of 10-cm wavelength, and the power profile is shown by the cross-hatched area at the right of the figure. The height profile of backscattered power agrees well with the profile of refractivity variance at the 20-cm sensor separation.

The bottom frame shows a tower experiment reported by Gossard et al. (1984a). Its goal was to compare radar-measured backscatter from very thin elevated layers, in which assumptions of isotropy

Figure A1 (opposite page). Top frame: Comparison of measured radar reflectivity (vertical axis) with the value calculated from refractometer-measured refractive index variance (horizontal axis) at the Bragg wavenumber k_r of the 10.7-cm-wavelength Wallops Island radar. The refractometer was suspended below a helicopter tracked by the radar. If Eq. (A4a) represents the correct physics of RIT scattering, the points should lie along the *solid* 45° line (Kropfli et al., 1968). Middle frame: Tower-measured height profiles of refractivity N and refractivity spatial variance ΔN_{20}^2 , obtained from a microwave refractometer with two cavities separated by 20 cm. The profile of backscattered power measured by a 10-cm-wavelength FM-CW radar is shown cross-hatched at the right (Bean et al., 1971). Bottom frame: C_n^2 within an elevated refractive layer (see radar display) measured with Lyman- α humidity and platinum wire temperature sensors at the 175-m height on a tower (bottom left) compared with the radar-measured height profile of C_n^2 (bottom right) using (A4a) to convert power to C_n^2 . The layer passed the 175-m level at 1814 MST (Gossard et al., 1984a).



and homogeneity are suspect, with in situ measurements of apparent C_n^2 obtained with fast-response platinum wire temperature sensors and a Lyman- α humidity sensor. The C_n^2 were calculated from point measurements of temperature and humidity using the known horizontal wind. Backscattered power was remotely measured with a vertically pointing 10.2-cm-wavelength FM-CW radar and converted to C_n^2 using (A4a). As the thin layer shown on the radar record rose past the 175-m fixed level on the tower, the records of C_q^2 and C_T^2 versus time were obtained, from which C_n^2 was calculated. The layer passed the 175-m level at about 1814 MST, and the radar-measured height profile of C_n^2 at that time is shown for comparison. The correspondence is good, lending considerable confidence that radar-measured values of "apparent" C_n^2 agree well with "apparent" C_n^2 values measured by the in situ sensors even within the thin layers of large height gradient. From the values of C_n^2 and C_w^2 measured as the layer rose past the 175-m level, and the values of dq/dz , $d\theta/dz$, and du/dz , measured by the dewpointer, quartz thermometer, and propyranes at the 150-m and 200-m fixed levels, the values of L_θ/L_w could be calculated from Eq. (1). The results are shown in Fig. A2.

A.2. REFRACTIVE INDEX OF MICROWAVE FREQUENCIES

For microwave frequencies, electromagnetic propagation through the atmosphere is essentially non-dispersive. The refractive index n is therefore independent of wavelength and is related to constituents of the air (e.g., Bean and Dutton, 1966) as

$$(n-1) \times 10^6 = 77.6 \left[\frac{p}{T} \right] + 3.73 \times 10^5 \frac{e}{T^2}, \quad (\text{A6})$$

which is often designated N and called the "refractivity" to distinguish it from n . The p is atmospheric pressure (mb), T is temperature (K), and e is vapor pressure (mb). We usually express humidity in terms of specific humidity q rather than vapor pressure, where q is the ratio of mass of water vapor to mass of moist air and is related to pressure and vapor pressure as

$$e = \left[\frac{p}{0.622 + q} \right] q \approx \frac{p}{0.622} q.$$

Because q is 3×10^{-2} or less, the approximation indicated is justified for nearly all applications. Thus, for practical purposes

$$N \approx \left[\frac{77.6p}{T} \right] \left[1 + \frac{7.73}{T} Q \right], \quad (\text{A7})$$

where Q is specific humidity in grams per kilogram of dry air; i.e., $Q = q \times 10^3$.

For the interpretation of clear-air radar backscatter, we are mainly concerned here with turbulence processes in which both heat and moisture are conserved. We usually assume no change of state (condensation or evaporation) and assume that parcel movements occur quickly enough so that temperature changes are essentially adiabatic, i.e., the parcel does not lose or gain heat by some process such as radiative transfer. For these problems it is very convenient to use potential refractivity ϕ (analogous to potential temperature), defined by

$$\phi = \frac{77.6p_r}{\theta} \left[1 + \frac{7.73Q}{\theta} \right], \quad (\text{A8})$$

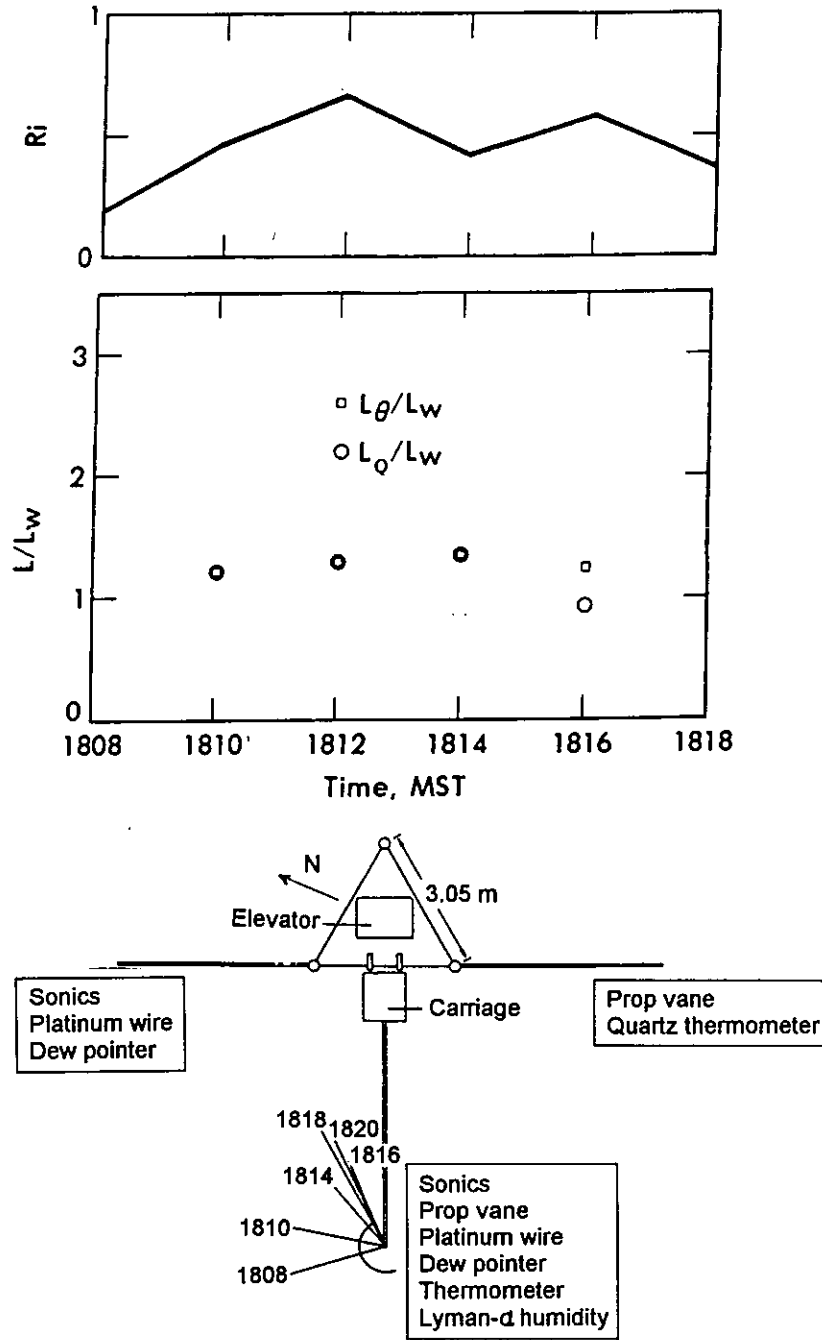


Figure A2. Top frame: Plot of Richardson number Ri from sensors at the 150-m and 200-m levels. Middle frame: L_θ/L_w and L_Q/L_w calculated from the left side of Eq. (1), using the measurements of C_θ^2 , C_Q^2 , and C_w^2 as the refractive layer rose past the 175-m level in the bottom frame of Fig. A1, and using the gradients of θ_0 , Q_0 , and u_0 found by differencing the values recorded at the 150-m and 200-m levels. It is seen that $L_\theta/L_w = L_Q/L_w = 1.3 \pm 0.1$. Bottom frame: Tower boom configuration, showing the exposure of sensors located on the boom ends. Note that the carriage sensors are contaminated by tower-generated turbulence after 1815 MST, 10 February 1982, as shown by the wind direction change indicated by the orientation of the time-labeled radial lines centered near the carriage. Until 1815 MST, the agreement of the measured L_θ/L_w and L_Q/L_w is extremely good.

where $\tilde{\theta}$ is potential temperature (K) for dry air given by

$$\tilde{\theta} = \tilde{T} \left[\frac{\tilde{p}_r}{\tilde{p}} \right]^{0.286}, \quad (\text{A9})$$

and p_r is some reference pressure level often chosen to be 1000 mb. The tilde is used for the total quantity to distinguish it from the unsubscripted perturbation component and the zero-subscripted mean used later in this section. We see that $\tilde{\phi}$ is the \tilde{N} value of a parcel moved from its ambient level to the reference level adiabatically without loss or gain of moisture. The conserved property, potential refractivity ϕ , is the convenient atmospheric parameter for most atmospheric science purposes, but of course the radar senses n .

The relationship between the variances of ϕ and n is

$$\overline{\phi^2} \approx \overline{N^2} \left[\frac{\tilde{p}_r}{\tilde{p}} \right]^{1.428} C^2, \quad (\text{A10})$$

where ϕ and N are deviations from the average. The primary difference between variances of ϕ and N is a height dependence entering because of the pressure factor. In the boundary layer, where $p \approx 1000$ mb, C is about one. At higher elevations Q/T generally becomes small and the conversion factor is almost entirely the pressure-height factor. Equations (A7) and (A8) show that height profiles of ϕ and N will differ substantially. If we define the potential refractive index relative to the local pressure-altitude at that height (instead of at the 1000-mb level), the pressure factors in (A9) and (A10) become unity; C_N^2 and C_ϕ^2 are seen to be virtually identical at that altitude.

A.3. RADAR SENSING OF THE GRADIENT QUANTITIES

Taking the derivative of $\tilde{\phi}$ in (A8), we find the linearized equation for small perturbations to be

$$d\tilde{\phi} = \frac{\partial \tilde{\phi}}{\partial \tilde{\theta}} d\tilde{\theta} + \frac{\partial \tilde{\phi}}{\partial \tilde{Q}} d\tilde{Q}, \quad (\text{A11})$$

where

$$\frac{\partial \tilde{\phi}}{\partial \tilde{\theta}} = - \frac{77.6 p_r}{\theta_0} \left[\frac{1}{\theta_0} + 15.46 \frac{Q_0}{\theta_0^2} \right] \equiv -a, \quad (\text{A12a})$$

$$\frac{\partial \tilde{\phi}}{\partial \tilde{Q}} = 77.6 p_r \left[\frac{7.73}{Q_0^2} \right] \equiv b. \quad (\text{A12b})$$

Figure A3 shows that a and b can be fairly accurately estimated from estimates of Q_0 and θ_0 based on standard atmospheres.

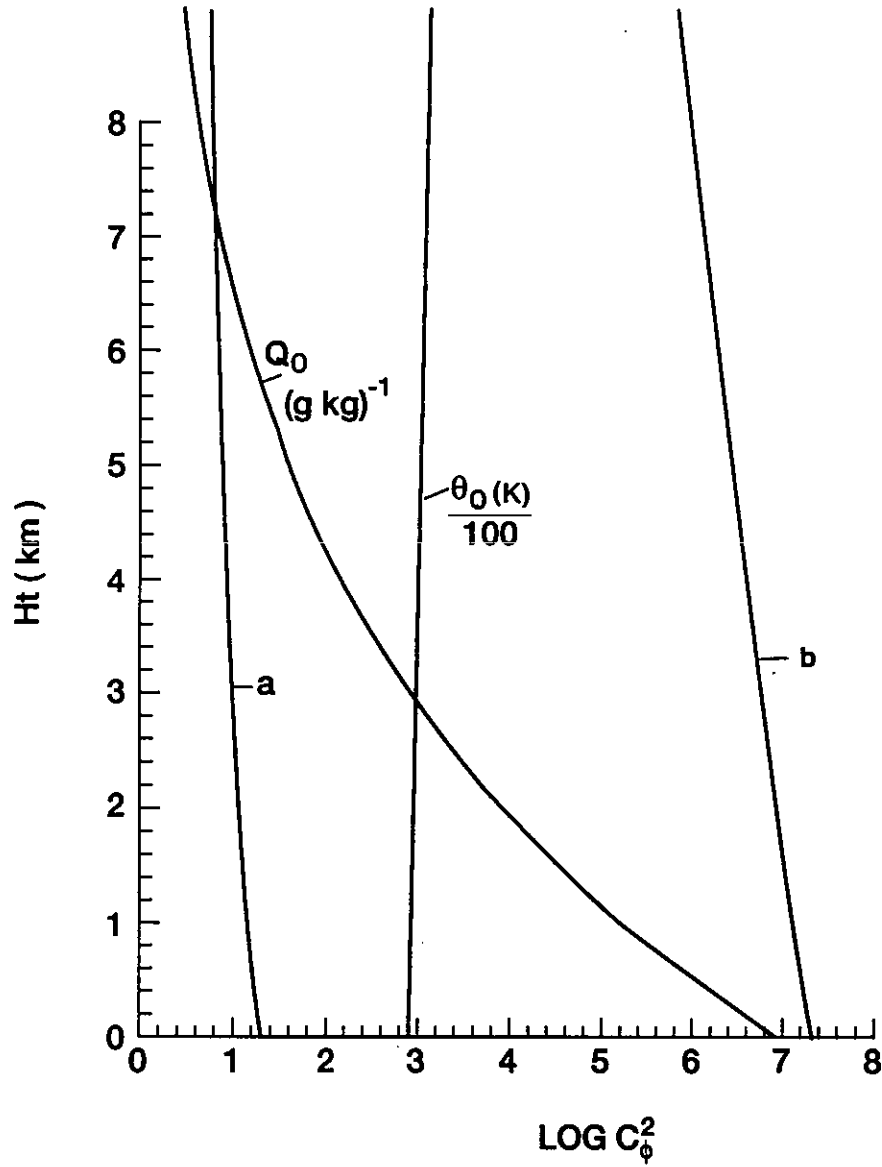


Figure A3. Height profiles of a and b [see Eq. (A11)] for quasi-standard atmosphere. Note that b changes by only 14% for $Q = 1$ to 7 g kg^{-1} .

In accord with our earlier convention, we let $d\phi = \phi$, $d\theta = \theta$, and $dQ = Q$ so that (A11) can be written $\phi = -a\theta + bQ$. Gossard (1960) pointed out, and Gurvich (1968) discussed, that the variance (and spectrum) of ϕ includes a temperature-humidity covariance (and cospectrum $\text{CO}_{\phi Q}$) term that can provide a large contribution (positive or negative according to the signs of the height gradients of θ_0 and Q_0) to the variance of refractive index. The effect has more recently been shown by Friehe et al. (1975), Wyngaard et al. (1978), and Hill (1978) to be important even in calculations of optical refractive index perturbation parameters. Thus

$$\overline{\phi^2} = a^2 \overline{\theta^2} + b^2 \overline{Q^2} - 2ab \overline{\theta Q} , \quad (\text{A13a})$$

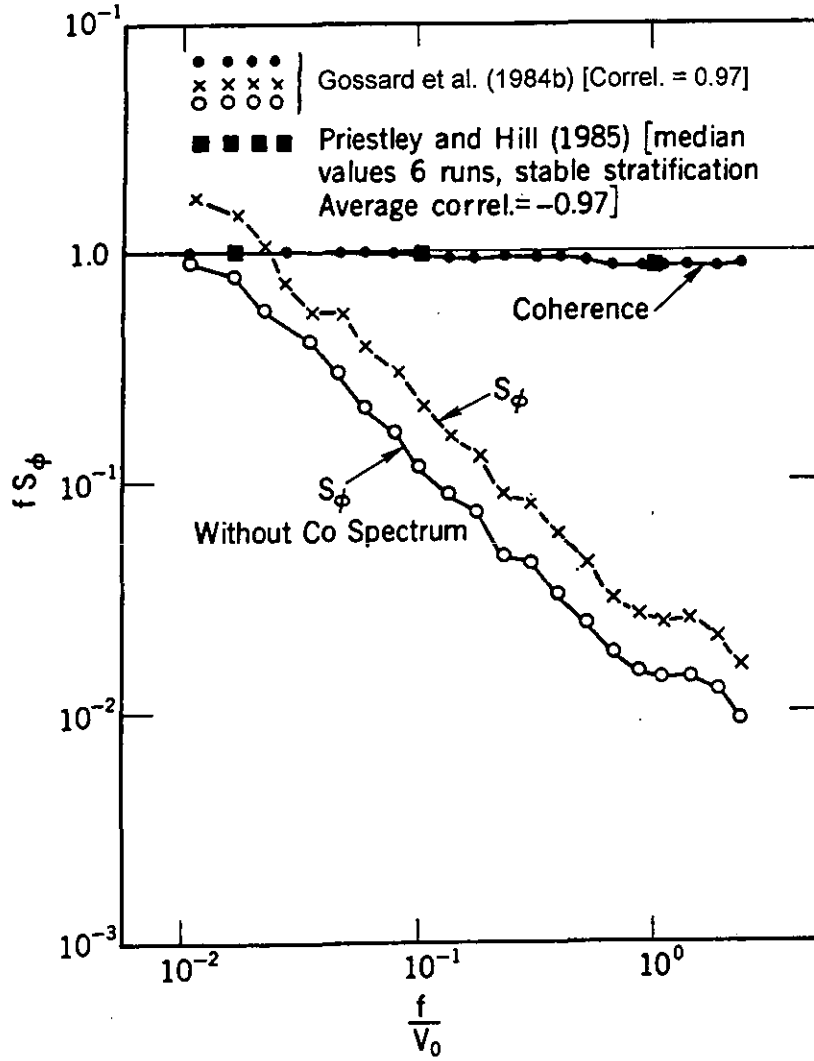


Figure A4. Spectra of potential radio refractivity, S_ϕ , within the stable elevated layer of 10 February 1982, described in Fig. A1 (bottom). The potential refractivity was calculated from (A13c) using Lyman- α measurements of humidity and platinum wire measurements of temperature. S_ϕ calculated with (crosses) and without (open circles) the cospectral contribution are shown. The contribution of the cospectrum is large because of the very high correlation (-0.97) between temperature and humidity; in fact, the temperature-humidity coherence (filled circles) is about 0.8 down to the smallest scales measurable in the experiment. A similar high correlation (-0.97) and coherence (filled squares) of temperature and humidity measured in the stable surface layer by Priestley and Hill (1985) are shown.

$$C_\phi^2 = a^2 C_\theta^2 + b^2 C_Q^2 - 2ab C_\theta C_Q, \quad (\text{A13b})$$

and

$$S_\phi(k) = a^2 S_\theta(k) + b^2 S_Q(k) - 2ab \text{CO}_{\theta Q}(k), \quad (\text{A13c})$$

where CO is the cospectrum of θ and Q .

To proceed much further, it is necessary to relate the spectrum S_ϕ to the spectral forms of S_θ and S_Q , and in particular to determine whether S_ϕ can be assumed to have the form (A3) within the ICS. This question has been argued affirmatively by Andreas (1987) and Hill (1989), and the correlation of θ and Q have been shown to be essentially unity under stratified conditions (see Fig. A4).

A.4. HUMIDITY RETRIEVAL

From (A11) it is clear that dQ/dz can be calculated from radar-measured $d\theta/dz$ if $d\theta/dz$ is known independently, say from RASS. So, in principle, profiler/RASS facilities can measure profiles of humidity gradient.